Nano Energy 76 (2020) 105085

Contents lists available at ScienceDirect

Nano Energy

journal homepage: http://www.elsevier.com/locate/nanoen

Atomically dispersed materials for rechargeable batteries

Zhiqi Zhang [a,1], Jiapeng Liu [a,1], Antonino Curcio [a], Yuhao Wang [a], Junxiong Wu [a], Guodong Zhou [a], Zhenghua Tang [d], Francesco Ciucci [a,b,c,*]

[a] Department of Mechanical and Aerospace Engineering, The Hong Kong University of Science and Technology, Hong Kong, China
[b] Department of Chemical and Biological Engineering, The Hong Kong University of Science and Technology, Hong Kong, China
[c] Guangzhou HKUST Fok Ying Tung Research Institute, Guangzhou, China
[d] Guangzhou Key Laboratory for Surface Chemistry of Energy Materials, New Energy Research Institute School of Environment and Energy, South China University of Technology, Guangzhou Higher Education Mega Centre, Guangzhou, China

ARTICLE INFO

Keywords:
Single atoms
Lithium metal batteries
Lithium-sulfur batteries
Sodium-sulfur batteries
Lithium-oxygen batteries
Zinc-air batteries

ABSTRACT

Rechargeable batteries have significantly helped to effectively use renewable energy sources as well as to intensively expand the electrification of vehicles. To achieve such goals, new advanced materials are urgently required. Atomically dispersed materials (ADMs) with single-atom metals supported on substrates feature uniform metallic sites and represent the utmost utilization of atoms, demonstrating wide applications in catalysis. These structural and morphological characteristics also make ADMs attractive materials for rechargeable batteries. Herein, we highlight and summarize the recent advances in synthetic methods for ADMs by physical confinement and chemical bonding. Subsequently, we summarize the recent progress in the design of diverse ADMs for lithium metal, lithium-sulfur, sodium-sulfur, lithium-oxygen, and zinc-air batteries and unveil the corresponding roles of ADMs from atomistic perspectives. Finally, the challenges and perspectives in this field are discussed.

1. Introduction

Global warming is one of the biggest challenges faced by humanity. To mitigate the impact of the abuse of fossil fuels, renewables are now being intensively developed. In this context, electrochemical energy storage (e.g. lithium-ion batteries, lithium-sulfur (Li–S) batteries, metal-air batteries, and supercapacitors) is an area of intense scientific research, where functional materials are the components that determine the performance [1,2]. It should be noted that finding materials capable of delivering simultaneously high energy density, stability, efficiency, and safety remains a significant challenge. To that end, nanomaterials have shown considerable promise [3]. For energy storage and conversion applications, metal nanoparticles supported on substrates are particularly attractive owing to the facile preparation, the merits of each individual component, and synergistic effects between the components. However, nanoparticles may coalesce. In addition, the larger the nanoparticle, the smaller the specific area is available for reactions. These two factors can significantly lower the activity. Downsizing the nanoparticles to make atomically dispersed materials (ADMs), i.e., atomically size metal atoms supported on substrates, could resolve both challenges. This strategy is particularly well suited for precious metals, which are often the best catalysts for various electrochemical reactions. In fact, the overall cost of ADMs might be lowered by decreasing the loading and improving the specific activity [4].

In catalytic reactions, ADMs have several advantages over conventional nanoparticles, including [5,6] i) an extraordinary catalytic activity and selectivity due to the unsaturated coordination sites of the active centers; ii) strong quantum-scale interactions between support and single-atoms (SAs); iii) a maximum utilization of all the atoms in a material that consequently minimizes costs; and iv) an improved understanding of catalytic reactivity mechanisms compared to nanoparticles due to the presence of well-defined active sites. To date, SAs have been constructed on several substrates, including carbons, carbon nitrides, boron nitrides, metals, metal oxides, nitrides, carbides, chalcogenides, and hydroxides [4,7–17]. Depending on the host materials, the physical and chemical properties of SAs change, providing many unique opportunities for tailoring SA-based catalysts [5,18]. For instance, Pt, Pd, or Ir SAs supported on non-conductive metal oxides

* Corresponding author. Department of Mechanical and Aerospace Engineering, The Hong Kong University of Science and Technology, Hong Kong, China.
E-mail address: francesco.ciucci@ust.hk (F. Ciucci).
[1] These authors contributed equally to this work.

https://doi.org/10.1016/j.nanoen.2020.105085
Received 24 March 2020; Received in revised form 9 June 2020; Accepted 14 June 2020
Available online 21 June 2020

have shown remarkable catalytic activity and selectivity towards CO oxidation, selective hydrogenation, and the water gas shift reaction [19–21]. Similarly, Pt or Pd SAs on poorly conductive carbon nitride have been used for the photocatalytic hydrogen evolution or hydrogenation reactions, respectively [10,22]. Carbon-supported SAs have found versatile applications in heterogeneous catalysis and electrochemical energy conversion [18,23–25]. In electrocatalysis, atomically-dispersed Pt anchored on carbon has proven to be active and stable towards hydrogen evolution reaction (HER) with a performance that is superior to the benchmark catalyst of commercial Pt/C [7]. In addition, atomically dispersed non-noble metals on nitrogen-doped carbon (M-N-C, where M = Fe, Co, Ni, Cu, Zn, etc.) have demonstrated an excellent oxygen reduction reaction (ORR) performance in both acidic and alkaline media [26].

The speed of the electrocatalytic reactions that occur during charge and discharge is critical to the performance of batteries. For example, the sluggish sulfur redox kinetics is one of the essential factors hindering the Li–S technology [27]. In an attempt to resolve this challenge, highly-efficient atomically dispersed electrocatalysts for the conversion of Li polysulfides (LiPSs) have been developed [28]. In the Li–O_2 and Zn-air battery systems, the electrocatalytic enhancement of the oxygen redox kinetics, i.e., ORR and oxygen evolution reaction (OER), is also crucial to improving the performance [29–31]. In Li-metal batteries, the growth and nucleation of dendrites can be prevented by using ADMs [32]. All these examples highlight that, while the field is at the beginning, ADMs have had an extremely promising application in rechargeable batteries. Here, we review how ADMs (mainly M-N-C electrode materials) have been i) synthesized; ii) characterized; iii) studied with atomistic calculations, including density functional theory (DFT); and iv) applied to Li-metal, Li–S, sodium-sulfur (Na–S), Li–O_2, and Zn-air batteries, see Fig. 1 for significant advancements in the field [29,30,32–34]. Challenges and perspectives will be also discussed at the end of this article.

2. Synthesis of ADMs

In this section, the most common synthetic approaches to make ADMs are overviewed (Fig. 2). We should note that due to their high surface free energy, SAs tend to aggregate, which is the biggest challenge for synthesis. Therefore, we will discuss how to strengthen the

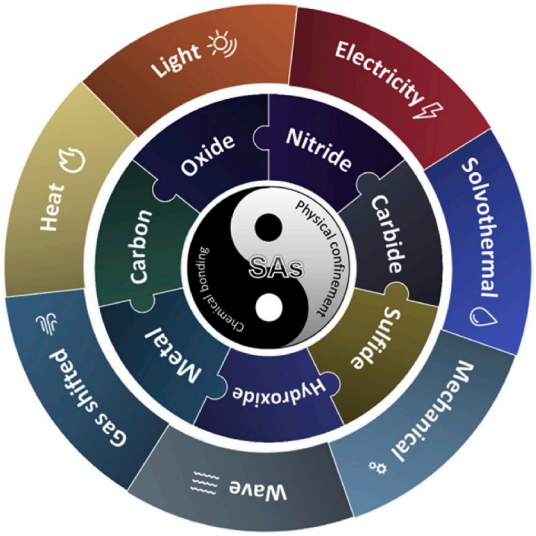

Fig. 2. Overview of the synthetic methods used for ADMs as discussed in this review.

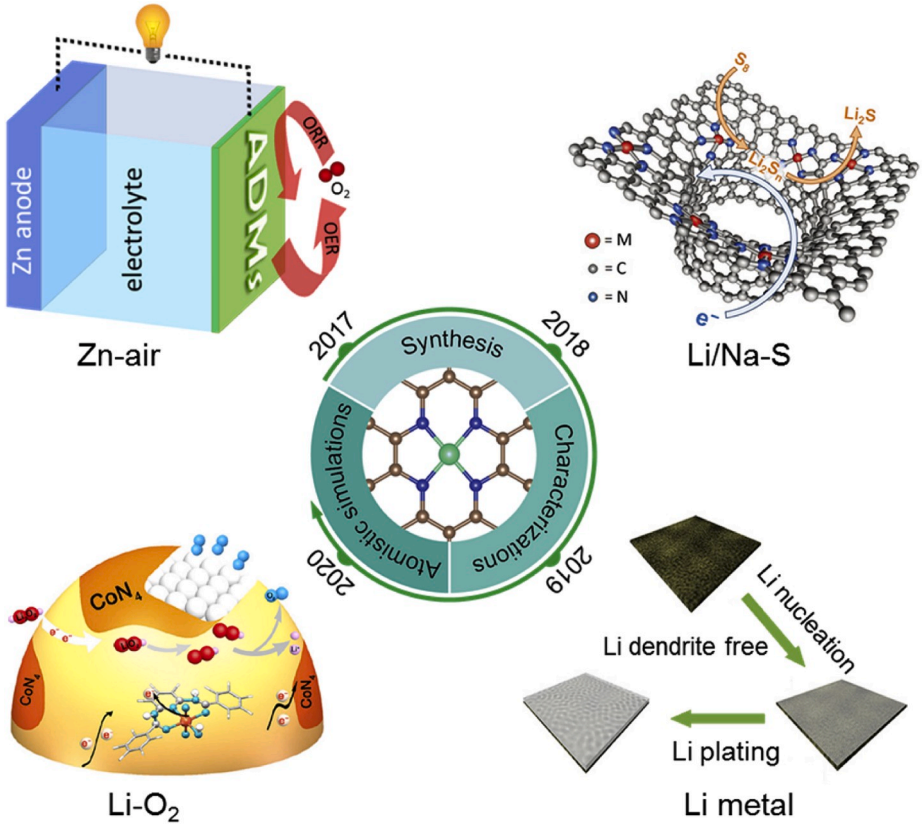

Fig. 1. Schematic illustration of ADMs applied to Li metal, Li/Na–S, Li–O_2, and Zn-air batteries. Reproduced with permission [32]. Copyright 2019, Wiley-VCH. Reproduced with permission [33]. Copyright 2017, Wiley-VCH. Reproduced with permission [30]. Copyright 2020, Nature Publishing Group.

interaction between metal and support so that the dispersed SAs are stabilized. A particular focus on physical confinement and chemical bonding will be given as both are the most effective strategies to trap and anchor SAs. Defects (e.g. vacancies) and micropores on the support materials are responsible for the physical confinement. Doping heteroatoms (e.g. N, O, and S) into the substrate to chemically bond to SAs is another workable approach to enhance the stability.

2.1. High-temperature pyrolysis

High-temperature pyrolysis has been proven to be an effective approach for the preparation of SAs. In fact, this method has been widely employed to make SAs of Pt [35], Ru [15,36], Fe [37], Co [38], Ni [39,40], Zn [41], and Mo [42]. The precursors, normally containing the target materials including SA-containing compounds, are first mixed and

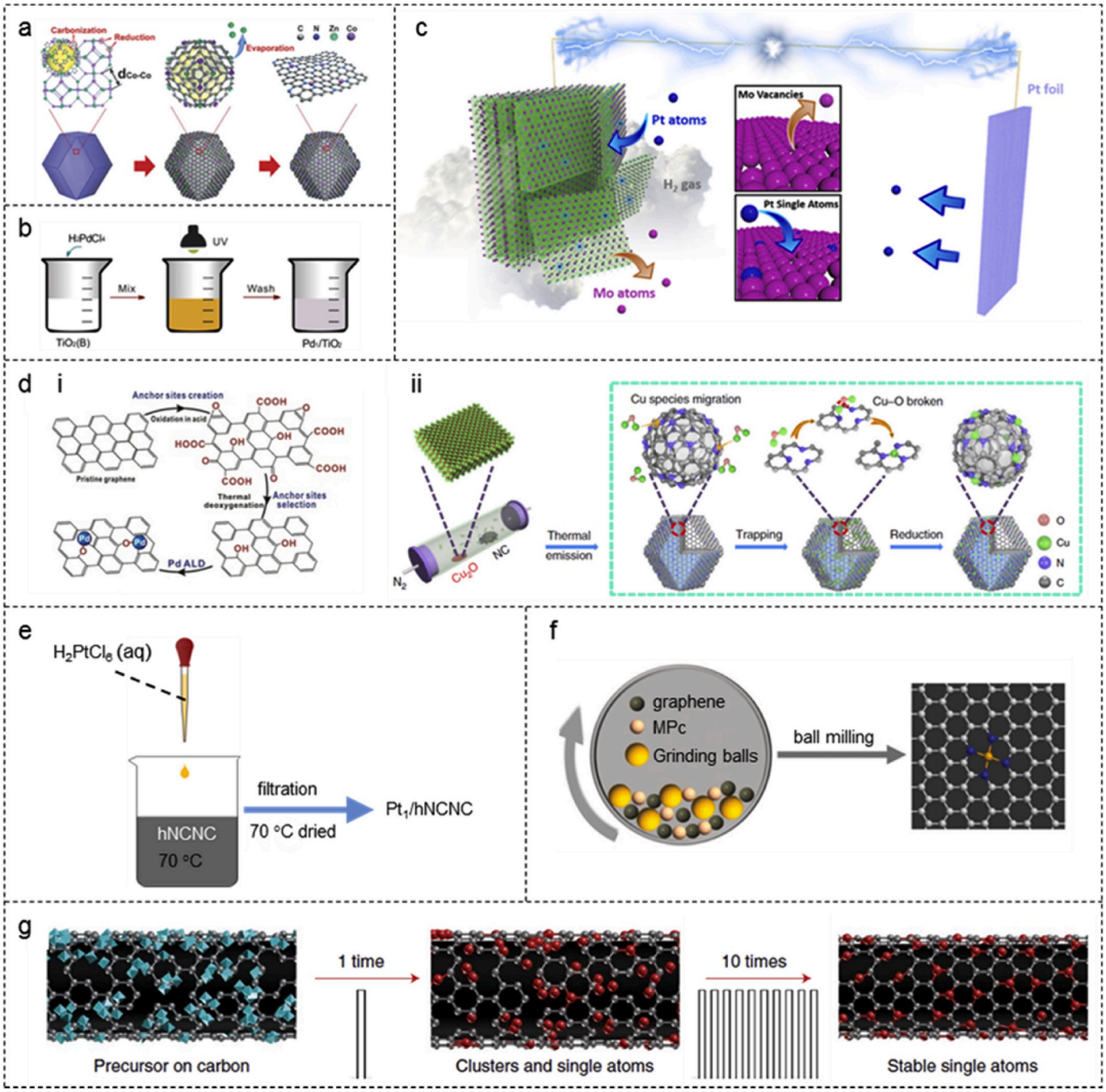

Fig. 3. Schematic illustration of the synthesis of ADMs. a) Construction of Co SAs on N-doped porous carbon by high-temperature pyrolysis of MOFs. Reproduced with permission [43]. Copyright 2016, Wiley-VCH. b) Construction of Pd SAs on TiO_2 by a photochemical route. Reproduced with permission [56]. Copyright 2016, The American Association for the Advancement of Science. c) Construction of Pt SAs on $Mo_2TiC_2T_x$ MXene nanosheet by electrochemical exfoliation. Reproduced with permission [65]. Copyright 2018, Nature Publishing Group. d) Gas-transport approach. i) Anchoring Pd SAs on the oxygen functional groups of graphene by ALD technique. Reproduced with permission [68]. Copyright 2015, American Chemical Society. ii) Construction of Cu SAs on nitrogen-rich carbon support with abundant defects. Reproduced with permission [71]. Copyright 2019, Nature Publishing Group. e) Construction of Pt SAs on hNCNC full of micropores. Reproduced with permission [7]. Copyright 2019, Nature Publishing Group. f) Construction of graphene-supported MN_x moieties by ball milling approach. Reproduced with permission [23]. Copyright 2019, Royal Society of Chemistry. g) Synthesis and dispersion of ADMs (grey, carbon atoms; cyan, metal precursor; red, metallic atoms) by a high-temperature-shockwave method. Reproduced with permission [81]. Copyright 2019, Nature Publishing Group.

then pyrolyzed typically at temperatures between typical 600 and 1100 °C. To make SAs supported by carbon-based materials, metal-organic frameworks (MOFs) [43–47], carbon black [35,41], graphene [36, 48–50], carbon nanotubes [51], polymers [52,53], glucose [40,54], chitosan [42,55], silk fibroin [38], and melamine [54] have been extensively employed. MOFs are the ultimate precursors for preparing ADMs. MOFs are made of transition metals bridged by organic linkers containing C and N atoms, that is, all the key elements for preparing SAs can be included in MOFs [45]. Plus the additional benefits that include the presence of abundant micropores and high surface areas, MOFs have been widely considered as ideal sacrificial templates to create SAs. Upon high temperature treatment, the metals can turn into SAs that are effectively anchored and/or confined in the linker-derived porous carbon-based hosts (Fig. 3a). Other carbon precursors, including graphene, glucose, and chitosan, lack the anchoring sites present in MOFs. Therefore, if these precursors are used, additives must be included so that the metal-support interaction can be improved upon carbonization. For example, urea can serve as a source of N that hybridizes with C during pyrolysis to form N-coordinating sites, which, in turn, facilitate the anchoring of SAs to the host material [35]. ADMs prepared by pyrolysis typically have high thermal stability. However, the high temperatures used usually require long preparation times and large amounts of energy.

2.2. Photochemical methods

ADMs can also be obtained by photochemical reduction. For example, Zheng and co-workers first introduced H_2PdCl_4 in an aqueous solution with TiO_2 and formed $PdCl_2$ on ethylene glycolate–stabilized ultrathin TiO_2 nanosheets. Then, Pd^{2+} ions were reduced by treating the samples under ultraviolet light (Fig. 3b) [56]. Wu and co-workers photochemically reduced a solution containing H_2PtCl_6 to Pt SAs solution at −40 °C [57,58]. Subsequently, they mixed the atomically dispersed Pt with mesoporous carbon, multi-walled carbon nanotubes, TiO_2 nanoparticles, and ZnO nanowires. It was suggested that the defects present in mesoporous carbon or the oxygen vacancies in TiO_2 were able to prevent the agglomeration of Pt SAs. Similarly, Pt SAs and clusters have been anchored on functionalized multiwall carbon nanotubes or MoO_2 by a light-mediated reduction of a mixture containing H_2PtCl_6 and the support material [59,60]. The photochemical synthesis of SAs can also be conducted in solids, as demonstrated by Liu et al. [61]. They firstly prepared the precursor powders consisting of adsorbed $[PtCl_6]^{2-}$ ions on an N-doped porous carbon material. After irradiating ultraviolet light onto the material for 1 h, the $[PtCl_6]^{2-}$ ions were transformed into Pt SAs. In this regard, defects contributed to the adsorption of $[PtCl_6]^{2-}$ ions. The reported examples only focus on noble-based ADMs. Therefore, whether photochemical methods can be applied to the preparation of non-noble ADMs still needs to be proven.

2.3. Electrochemical methods

By carefully controlling the electrolyte concentration, deposition time, current, and potential, SAs can also be prepared through electrodeposition. It is well known that, for HER in acid media, if Pt wire is employed as the counter electrode, Pt can be dissolved and transferred to the cathode to form Pt nanoparticles on carbon, leading to an artificial HER performance enhancement [62]. Inspired by this phenomenon, Laasonen et al. obtained pseudo-atomic-scale Pt on single-walled carbon nanotubes (SWNTs) by cycling the potential between −0.55 and 0.25 V vs. the reversible hydrogen electrode (RHE). Pt species are firstly dissolved in sulfuric acid from a Pt foil counter electrode and then electrochemically adsorbed on a working electrode consisting of SWNTs [63]. Similarly, Luo et al. were able to synthesize large-area and binder-free Pt SAs on CoP-based nanotube arrays supported by a Ni foam. Such Pt SAs were obtained by simply cycling in a three-electrode cell containing a phosphate buffer solution [64]. This approach suggests that combining physical confinement at surface vacant sites and chemical bonding with C atoms is a promising strategy to scale-up the production of ADMs. Wang and co-workers immobilized Pt SAs on the surface Mo vacancies of $Mo_2TiC_2T_x$ MXene via electrochemical exfoliation. The latter process was done by cycling the potential between 0 and -0.6 V (vs. RHE) at a scan rate of 20 mV s^{-1} in a 0.5 M H_2SO_4 (Fig. 3c) [65]. Note that, the Pt–C bonds, originating from the interaction of Pt with C atoms on the MXene, are beneficial for the stability of Pt SAs. Electrochemical methods can also be used to make non-noble metal-based ADMs. Li and co-workers fabricated isolated Ni and Fe atoms anchored on graphdiyne by electrochemical deposition [66]. Graphdiyne was first immersed in an aqueous solution containing $NiSO_4$ or $FeCl_3$ to allow the adsorption of Ni or Fe. Subsequently, the Ni or Fe SAs were electrodeposited galvanostatically at a current density of 10 mA cm^{-2}. We must note that there are two shortcomings with this type of preparation method. First, the substrates used for the electrochemical preparation of ADMs need to be good electronic conductors. Second, electrodeposition only occurs where the surface of the electrode is in direct contact with the electrolyte, potentially leading to insufficient dispersion.

2.4. Gas-transport synthesis

Gas-transport synthesis leverages the transportation (through the gas phase) and deposition (onto solid substrates) of atomic metal precursors. Relevant techniques include atomic layer deposition (ALD), chemical vapor deposition, and mass-selected soft landing. The Sun group deposited SAs and clusters of Pt on nitrogen-doped graphene nanosheets (GNs) using several ALD cycles with trimethyl(methylcyclopentadienyl) platinum ($MeCpPtMe_3$) and O_2 as precursors [67]. The N-dopant sites were believed to be responsible for the stabilization of both Pt atoms and clusters. The Lu group fabricated Pd SAs on graphene using a palladium hexafluoroacetylacetate ($Pd(hfac)_2$) precursor. By controlling the amount of oxygen functional groups on graphene during ALD, Pd SAs were immobilized, and hfac ligands could be removed (Fig. 3d) [68]. Recently, the same group deposited Pt_2 dimers ($MeCpPtMe_3$ was the precursor) on graphene support that was decorated with phenol-related oxygen anchor sites by ALD [69]. We should note that the SA loading achieved by ALD is, typically, relatively low. For example, in the work of Yan and co-authors, only 0.25 wt% of Pd SAs were dispersed on graphene [68]. Wu and co-workers developed a gas-transport strategy for transforming bulk metals and metal oxides directly into SAs [70–72]. In this process, the bulk precursors were firstly turned into a gas and subsequently adsorbed onto the surface of a highly defective N-rich carbon support. In one representative work, Wu and colleagues heated Cu_2O and nitrogen-doped carbon at 1000 °C in a stream of N_2 [71]. Cu_2O sublimated into a vapor and was subsequently trapped and reduced by the defect-rich nitrogen-doped carbon, finally forming isolated SAs of Cu. It is worth emphasizing that both the physical confinement of defects and the chemical bonding of O or N-dopants are also responsible for stabilizing SAs. We should point out that conversion of the metal precursors from the solid to the gas state usually requires high temperatures, which are also energy consuming.

2.5. Solvothermal method

The above methods are mostly associated with harsh conditions (high or ultralow temperatures or darkroom conditions), expensive equipment, designated precursors, or complicated preparation processes. These issues can be eliminated by using the solvothermal methods, which have been extensively employed for preparing nanomaterials and SAs. A notable advantage is that solvothermal methods only require temperatures typically below 200 °C. Further, SAs can be well immobilized on different supports, including carbon [7], C_3N_4 [10, 22], sulfides [12], hydroxides [13,14], and MOFs [73]. Such supports, which are abundant in defects and heteroatoms, favor the confinement

and adsorption of SAs and enhance the metal-support interaction. Hu et al. developed hierarchical 3D N-doped carbon nanocages with micropores (~0.6 nm). This particular material has the unique advantage of combining the physical confinement of nanopores and the chemical bonding of N (Fig. 3e) [7]. Specifically, both the $[PtCl_6]^{2-}$ anions (~0.5 nm) and dechlorinated Pt SAs can be trapped in the micropores with a larger Gibbs free energy of adsorption compared to that of the graphitic plane. The N defects further decrease the Gibbs free energy of adsorption, leading to improved stabilization of the $[PtCl_6]^{2-}$ anions and Pt SAs. Using this strategy, a series of Pt (with a loading of 5.68 wt%), Pd, Au, and Ir SAs have been immobilized on hierarchical N-doped carbon nanocages (hNCNCs). Considering that these materials are prepared under mild conditions, it still needs to be proven whether they can work stably at high temperatures. In fact, these SAs have been shown to suffer from aggregation at 300 °C [7].

2.6. Ball-milling

High energy ball-milling is another straightforward means to produce and modify nanomaterials [74–76]. Deng and co-workers synthesized various transition metal (Mn, Fe, Co, Ni, and Cu) SAs embedded into a matrix of GNs by high-energy ball milling the corresponding metal phthalocyanine (MPc) precursors and GNs. These materials can serve as efficient catalysts for benzene oxidation, dye-sensitized solar cells, methane conversion, and ORR (Fig. 3f) [77–80]. During the high energy ball-milling process, defects were introduced into the graphene network, while MPc was destroyed and turned into isolated MN_4 (M = Mn, Fe, Co, Ni, and Cu) centers. Subsequently, MN_4 bonded with graphene at defect sites, and this bonding led to a reconstruction of the carbon framework. Ball-milling is suitable for the large-scale fabrication of ADMs. However, two issues with this approach are the uneven dispersion of SAs and the difficulty in controlling the energy supplied during the process [25].

2.7. Wave-assisted methods

SAs can also be created by wave-assisted approaches, including shockwave, sonication, and microwave methods. Recently, Hu and co-workers reported that shockwaves can be used as a universal method for the construction of Pt, Ru, and Co SAs on various substrates, including carbon, C_3N_4, and TiO_2 (Fig. 3g) [81]. The high temperature of the shockwaves provided the activation energy required to form the SA dispersion. Thanks to the thermodynamically stable metal–defect bonds, the obtained catalyst demonstrated superior stability in direct methane conversion for 50 h. SAs such as Pd and Pt can be attached to the S sites of the basal plane of 1T-MoS_2 by the sonochemical reduction of the metal precursors in either water or isopropanol at room temperature [82]. Besides reducing the metal precursors, sonication can also be used to extract SAs from the bulk metals. For instance, if a graphene oxide (GO) slurry and a Fe, Co, Ni, or Cu metal foam are mixed and dried at ambient conditions, electron transfer occurs from the metals to the dangling bonds of the oxygen groups on GO, leading to the formation of M − O (M = Fe, Co, Ni, or Cu) bonds [83]. Specifically, the single metal atoms can be stripped from the metal foam by the M − O bonds with the assistance of sonication. Microwave heating is also an effective approach for fabricating highly dispersed nanoparticles because of its simplicity and high efficiency, particularly when used on heteroatom-doped supports [84,85]. By fine-tuning the reaction conditions, the metal-support interaction can be adjusted to reduce the size of the nanoparticles. Duan and co-workers first introduced metal precursors (Co, Cu, or Ni salt) in an amine-functionalized GO solution, the mixture was subsequently freeze-dried, after microwaving at 1000 W for 5 s within an Ar-filled glove box, the SAs on nitrogen-doped graphene (NG) were finally obtained [86].

It is worth mentioning that some ADMs were prepared by combining two or several of the above strategies together. For rechargeable batteries, high-temperature pyrolyzed M-N-C has several advantages such as i) a strong coordination between the N sites and the metals impart the SAs with robust stabilization that the SAs can be well preserved during various electrochemical energy storage processes; ii) the abundant reserves of transition metals and plentiful choices for precursors dramatically lower the preparation cost compared with noble-metal-based materials; and iii) the N-doped carbon substrates usually have good electrical conductivity and large surface area, which are favorable for the electrochemical energy storage.

3. Characterization of ADMs

Understanding the morphology, structure, and metal-support interaction is critical to the investigation of ADMs. Thanks to the rapid development of cutting-edge characterization, it is now possible to probe materials down to the atomic scale. Recent advances in sophisticated characterization methods, including high-angle annular dark-field imaging scanning transmission electron microscope (HAADF-STEM), scanning tunneling microscopy, synchrotron radiation-based X-ray absorption spectroscopy (XAS), Fourier-transform infrared spectroscopy, nuclear magnetic resonance, can precisely locate the individual metal atoms and provide direct local structural information about SAs and their supports [26]. For example, HAADF-STEM can be used to see individual metal atoms and determine their spatial distribution. Heavier single metal atoms can often be identified by a greater brightness than the support, allowing an estimation of the atomic density and distances. XAS, including X-ray absorption near edge structure (XANES) and extended X-ray absorption fine structure (EXAFS) spectroscopy, can provide the information complementary to that of HAADF-STEM [26]. For instance, XAS has been performed to evaluate the chemical structure of ADMs, and XANES had been used to evaluate the electronic state of metal atoms. Further, by fitting the EXAFS spectrum, one can establish the local chemical environment of ADMs, including coordination number, distances between absorbed, backscattered, and adjacent atoms. It is worth mentioning that, in some cases, fitting the EXAFS is difficult and might lead to ambiguous results. First-principle computations, including density functional theory, have been developed on the basis of the XAS results to achieve in-depth structural information, including the coordination of metal centers [87].

4. Applications of ADMs in batteries

ADMs hold great advantages in battery applications, as they possess unique coordination characteristics and active sites, and can provide unique Li/Na nucleation sites in Li or Na metal batteries, allowing the realization of high capacity cells. Moreover, ADMs can promote several critical electrocatalytic reactions, including OER or ORR. In particular, their use in electrodes and solutions has improved the performance and stability of Li–S/Na–S, Li–O_2, and Zn-air batteries. In this section, we will review how ADMs provide new avenues for the optimization of advanced energy storage materials.

4.1. Lithium metal batteries

Li batteries have been widely investigated in the past decades. Li metal electrode has the highest specific capacity (3860 mAh g^{-1}) and the lowest electrochemical potential (−3.04 V vs. standard hydrogen electrode) among all the electrodes [88–91]. Unfortunately, the use of untreated Li-metal electrodes leads to the growth of Li dendrites, which are responsible for internal short circuits, low Coulombic efficiencies (CEs), and shortened cycle lives of Li batteries [92]. Furthermore, Li dendrites constitute a very serious safety hazard. To solve these issues, tremendous efforts have been devoted to modifying electrolytes, solid electrolyte interphase layers, and electrodes, as summarized in a recent review [92].

The distribution and growth of dendrites are influenced by the sites where they nucleate and grow [93]. One promising approach to

suppress dendrites is to design Li metal hosts. In this context, carbon-based materials have been widely studied due to their high conductivity, extraordinary stability, and low costs. Cui and co-workers designed Au nanoparticles encapsulated in carbon shells as seeds for lithiation and found that the overpotential for Li metal deposition is close to 0 V vs. Li/Li^+. The Li metal nucleated around Au seeds and enclosed with a carbon shell effectively blocks the growth of Li dendrites [94]. This strategy improved the cycle stability and led to a 98% CE during the first 300 cycles. Following this concept, Yan and co-workers dispersed single-cluster Au supported by a carbon cloth (SCAu-CC), which physically constrained the growth of dendrites (Fig. 4a) [95]. The resulting Li anode exhibited an areal capacity of 20.0 mAh cm^{-2} and a CE of 99.82% for over 900 cycles at 1 mAh cm^{-2}. Gong and co-workers constructed SAs of Ni, Pt, and Cu supported on an NG matrix as stable hosts for the deposition of metallic Li [32]. Both the lipophilicity of the electrode surface and the atomic structural stability of the Li host were improved due to the presence of the metal atomic sites, see Fig. 4b. The working electrode consisting of atomically dispersed Ni on NG (SANi-NG) showed a homogenous and dendrite-free Li deposition throughout the electrode. In addition, SANi-NG had an ultralow voltage hysteresis of 19 mV, an average CE of 98.45% over 250 cycles, and a stable Li plating/stripping performance even at a high current of 4.0 mA cm^{-2} (Fig. 4b). Similarly, Yan et al. reported the use of Fe SAs decorated N-doped carbon matrix (Fe_{SA}-N-C) as lithiophilic sites for Li nucleation [96]. Fe_{SA}-N-C exhibited a much lower nucleation overpotential (0.8 mV) than pristine carbon (18.6 mV) due to the affected electron cloud around C by the combined Fe SAs and N. As shown in Fig. 4c, such extremely low overpotential impeded the growth of lithium dendrites. Consequently, the Fe_{SA}-N-C@Cu electrode could reach a CE of 98.8% for nearly 200 cycles in Fe_{SA}-N-C@Cu||Li cells and extend the cycle life of high-specific-capacity Li-metal batteries beyond that of cells with C@Cu electrodes. Apart from carbon-supported SAs, Yang et al. made a dendrite-free Li metal electrode by immobilizing Zn SAs on MXene ($Ti_3C_2Cl_x$) (Zn-MXene) [97]. In this material, Li nucleates homogeneously due to the presence of the lithiophilic Zn atoms. Moreover, the integration of Zn SAs and MXene led to a low overpotential of 11.3 ± 0.1

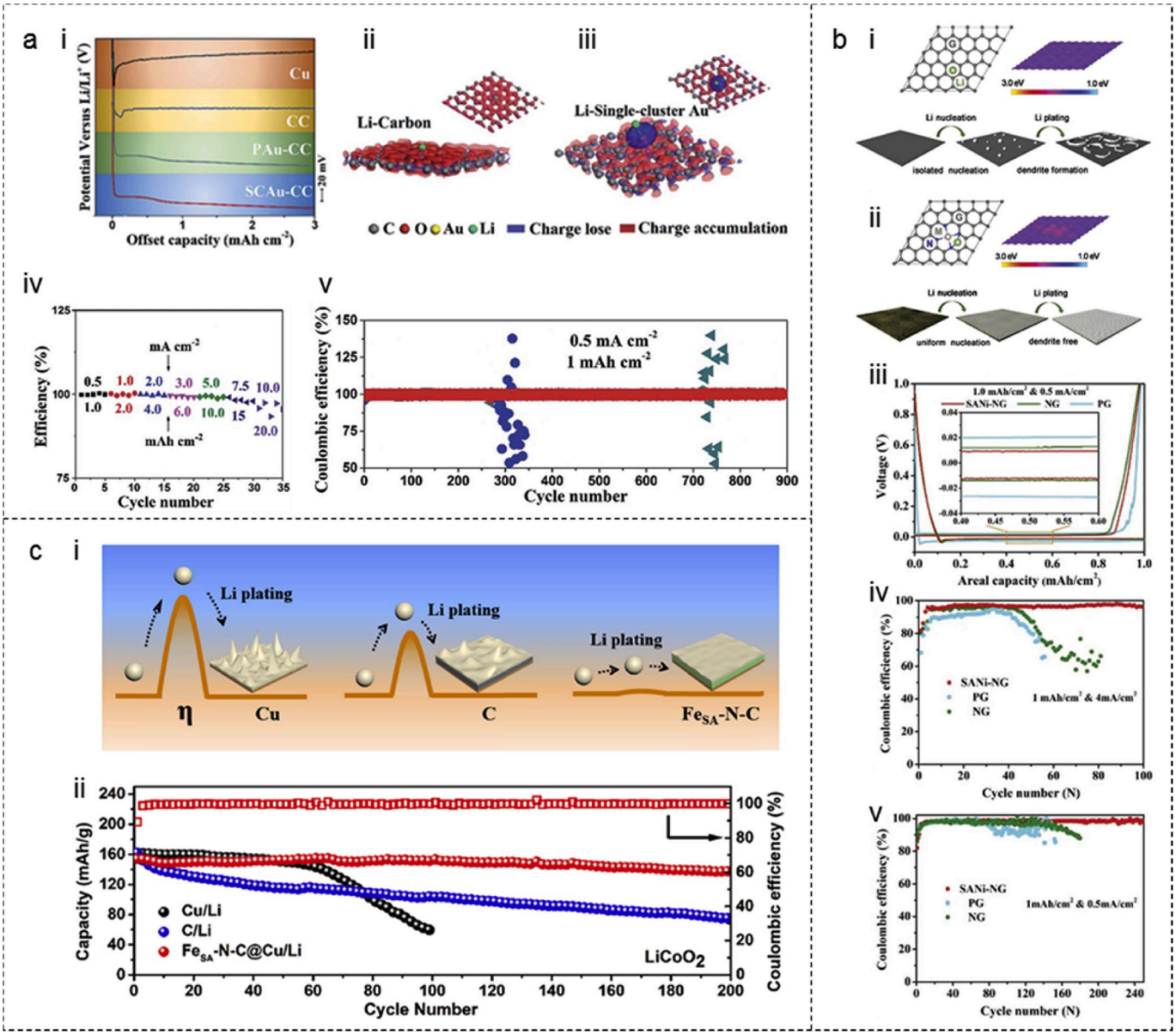

Fig. 4. Lithium anode decorated by ADMs or a single cluster. a) SCAu-CC for lithium anode. Reproduced with permission [95]. Copyright 2019, Royal Society of Chemistry. b) SANi-NG for lithium anode. Reproduced with permission [32]. Copyright 2019, Wiley-VCH. c) Fe_{SA}-N-C for lithium anode. Reproduced with permission [96]. Copyright 2019, American Chemical Society.

mV, a long cyclic life (1200 h), and deep stripping-plating levels up to 40 mAh cm^{-2}.

4.2. Li/Na–S batteries

Li–S batteries can potentially supplant conventional Li-ion batteries, due to their higher theoretical energy density (2600 Wh kg^{-1} vs. ~300 Wh kg^{-1}) and specific capacity (1672 mAh g^{-1} vs. 372 mAh g^{-1}) [27, 98]. One additional advantage is that S resources are abundant and cheap. However, the Li–S battery technology is hindered by several critical challenges, including i) a low utilization of S; ii) a significant volume change (~80%) occurring during cycling that can severely damage the electrodes; and iii) the shuttle effect of LiPSs, which leads to the corrosion of the Li anode, low CEs, and an irreversible capacity degradation during cycling. In the past two decades, tremendous research efforts have aimed at immobilizing the LiPSs in the cathode. Such an immobilization has been achieved by physically confining the S-containing compounds within porous carbon-based materials and by promoting the chemical interaction of LiPSs with polar species [28]. Unfortunately, the weak interaction between LiPSs and non-polar carbon is unable to effectively trap the soluble LiPSs generated during S reduction, thus leading to the loss of S in the cathode and LiPS shuttling.

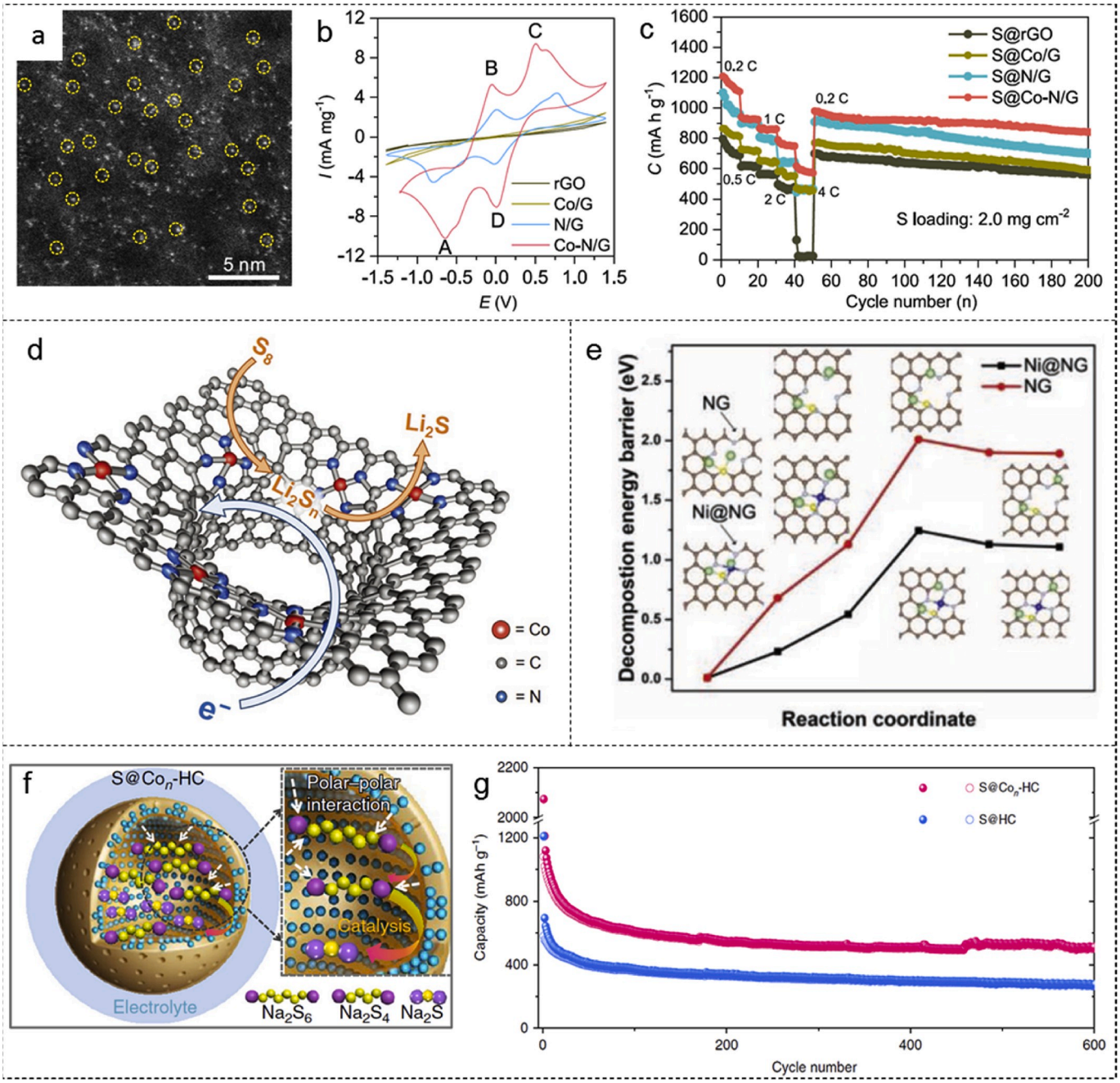

Fig. 5. a) HAADF-STEM image of Co–N/G. b) and c) Electrochemical performance of an Li–S battery with Co–N/G and related control samples: b) cyclic voltammograms of symmetric cells and c) rate capabilities. Reproduced with permission [105]. Copyright 2019, American Chemical Society. d) Schematic representation of SC-Co. Reproduced with permission [33]. Copyright 2019, Wiley-VCH. e) Decomposition energy barriers of Li_2S on the Ni@NG and NG (Blue, cyan, green, yellow, and brown balls represent Ni, N, Li, S, and C atoms, respectively). Reproduced with permission [40]. Copyright 2019, Wiley-VCH. f) Schematic illustration of the electrode reaction mechanism of NaPSs in S@Co_n-HC. g) Cycling performance of S@Co_n-HC and S@HC. Reproduced with permission [34]. Copyright 2018, Nature Publishing Group.

We should note that the generated LiPSs can inevitably diffuse across the cells because of the concentration gradients, and such a situation could be even worsened with the increase of sulfur loading and sulfur/electrolyte ratio.

Accelerating the conversion kinetics of soluble LiPSs to insoluble Li_2S_2/Li_2S has been proposed to resolve the shuttle problem. Highly-efficient LiPS conversion with enhanced reaction kinetics could be obtained using various catalysts, including metal nanoparticles [99–101], metal oxides [102], metal sulfides [103], and metal nitrides [104]. Recently, ADMs have been employed for expediting the LiPS conversion. Kong and co-workers developed atomically dispersed cobalt atoms embedded in the nitrogen-doped graphene framework (Co–N/G) to catalyze the electrochemical conversion of LiPSs (Fig. 5a) [105]. The Co–N–C coordination centers facilitate both the formation and decomposition of solid Li_2S during both the charging and discharging process (Fig. 5b). DFT calculations show that energy barriers of oxidation/reduction of Li_2S are reduced on Co–N/G. As a result, the S@Co–N/G composite, with a high S mass ratio of 90 wt%, delivered a gravimetric capacity of 1210 mAh g^{-1} along with an areal capacity of 5.1 mAh cm^{-2} (Fig. 5c). Also, the S@Co–N/G composite had a capacity fading rate of 0.029% per cycle over 100 cycles at 0.2 C with an S loading of 6.0 mg cm^{-2}. Huang et al. developed a highly-polar and electrocatalytically active material by implanting atomic Co into a mesoporous carbon material (SC–Co) (Fig. 5d) [33]. The open mesoporous channels allowed the LiPSs to access the electrochemical interfaces, including the Co atoms. Meanwhile, the atomic Co could improve the interaction with LiPSs and the kinetics of the sulfur redox reactions as well as preserve the mesoporous structure. Consequently, the Li–S batteries demonstrated a high CE and discharge capacity (837 mAh g_S^{-1} at 0.5 C) and were stable for 300 cycles with a low decay rate of 0.086% per cycle.

ADMs have been employed not only in cathodes but also in separators and electrolytes. Niu and co-workers modified the separator by coating Ni SAs embedded in NG thin layers (Ni@NG) using tape casting [40]. The Ni–N_4 motif in Ni@NG provided active Ni centers and facilitated the LiPS conversion by trapping and kinetic enhancement, as shown in Fig. 5e. Therefore, the Li–S batteries based on the Ni@NG modified separator had excellent rate performance and cycling stability with only a 0.06% capacity decay per cycle at 10.0 C. Xie and co-workers modified the separator of commercial polypropylene by coating Co, Ni, and Fe SAs on NG materials [106]. The Fe-SA-modified separator outperformed the other samples in blocking the crossover of polysulfides and improving their redox kinetics. The corresponding Li–S batteries, which were characterized by a relatively high sulfur loading of ~4.5 mg cm^{-2}, retained 83.7% of their initial capacity after 750 cycles at 0.5 C. Yang et al. used first-principle calculations to design cobalt hexadecachlorophthalocyanine (CoPcCl), a cobalt hexadecachlorophthalocyanine ramification. CoPcCl is a soluble ADM that is characterized by an excellent dispersibility, an inability to be covered by solid reaction products, and good redox activity with LiPSs. In light of these properties, CoPcCl, even at the 0.1 wt% level, significantly promoted the conversion of LiPSs [107].

Room temperature (RT) Na–S batteries are projected to be even more cost-effective and deployable on a larger scale than Li–S batteries [108, 109]. Theoretically, RT Na–S batteries are characterized by similar reaction mechanisms as in Li–S batteries and consequently have rapidly decaying capacities [110]. By using atomic Co-decorated hollow carbon nanospheres as a S host (S@Co_n-HC), Chou and co-workers were able to enhance the sodium polysulfides (NaPSs) conversion and boost the capacity and stability of RT Na–S batteries (Fig. 5f) [34]. The obtained sulfur cathode delivered an initial reversible capacity of 1081 mA h g^{-1} with 64.7% sulfur utilization rate. Remarkably, the cell retained a high reversible capacity of 508 mA h g^{-1} at 100 mA g^{-1} after 600 cycles (Fig. 5g). Table 1 reports the electrochemical performance of ADMs for Li/Na-based batteries.

4.3. Metal-O_2/air batteries

Metal-O_2/air batteries, such as Li–O_2 and Zn-air batteries, are also regarded as promising candidates for the next generation of electric vehicles owing to their high theoretical energy density and low cost [31, 115]. Regarding Li–O_2 batteries, at the cathode side, oxygen is firstly reduced and then released upon reiterative discharge and charge. This process is accompanied by the formation and decomposition of lithium peroxide (Li_2O_2) [116]. However, the insoluble and insulating Li_2O_2 leads to weak performance, including a low roundtrip efficiency, low rate capability, and poor cycling stability [116]. Several electrocatalytic materials, including carbonaceous materials, noble metals, metal oxides, and sulfides, etc., have been used to improve the oxygen redox kinetics and thus reduce the large overpotential between ORR and OER. However, these materials still suffer from severe shortcomings, such as high cost and scarcity, along with their poor durability and relatively low capacity [29,30]. Recently, the Yin and Xu group developed carbon-supported Co SAs to address these issues [29,30]. Yin et al. fabricated 2D nitrogen-rich carbon nanosheets coordinated with isolated Co-N_x active sites (Co–SAs/N–C) for Li–O_2 batteries (Fig. 6a) [29]. These authors found that the Co-N_x in Co–SAs/N–C enhanced the LiO_2-absorption ability and thus modulated the growth and distribution of Li_2O_2 so that its size could be 2–3 nm during the ORR (Fig. 6b and e). During the ORR of the control samples, which did not contain Co–N_4 but consisted in either Co nanoparticles trapped in N-rich carbon (Co-NPs/N–C) or N-doped carbon nanosheet (N–C), the Li_2O_2 aggregated into particles in the sizes of 100–300 nm (Fig. 6c, d and 6f). In turn, the Co-N_x moieties can easily decompose the 2/3-nm-sized Li_2O_2. As expected, the Co–SAs/N–C electrode have an ultra-low charge/discharge polarization (0.40 V), a high rate discharge capacity (11,098 mAh g^{-1} at 1 A g^{-1}) and an excellent cyclability (260 cycles at 400 mA g^{-1}) (Fig. 6g). Similarly,

Table 1
The electrochemical performance of state-of-the-art Li/Na batteries using ADMs.

Sample	Battery	Content of metal	Loading (mg cm^{-2})	Current density (mA cm^{-2})	Overpotential (mV)	Cycle	Capacity (mAh g^{-1})	Ref.
SANi-NG	Li metal	0.48 at%	0.7	4.0	–	250	–	[32]
SCAu-CC	Li metal	–	2.6	3.0	0	200	116 ($LiFePO_4$)	[95]
Fe_{SA}-N-C	Li metal	–	–	1	0.8	200	137 ($LiCoO_3$)	[96]
Zn-MXene	Li metal	0.87 at%	–	1	11.3	500	100 ($LiFePO_4$)	[97]
Ni@NG	Li–S	–	1.5	–	–	500	826	[40]
Co–N/G	Li–S	0.77 at%	6.0			100	1175	[105]
SC-Co	Li–S	0.72 wt%	1.2	–	–	300	837	[33]
Fe SAs on NG	Li–S	0.54 at%	4.5	–	–	750	746	[106]
Co–SAs@NC	Li–S	0.66 wt%	3.81	–	–	600	737	[111]
C–C–N–Co	Li–S	4.1 wt%	1.0	–	–	100	787	[112]
FeSA-CN/S	Li–S	1.14 wt%	2.4	–	–	500	605	[113]
CoPcCl electrolyte additive	Li–S	0.1 wt%	1.16	–	–	200	831	[107]
Co@C_3N_4	Li–S	–	4.0	3.2	–	200	980	[114]
S@Co_n-HC	Na–S	7.06 wt%		–	–	600	508	[34]

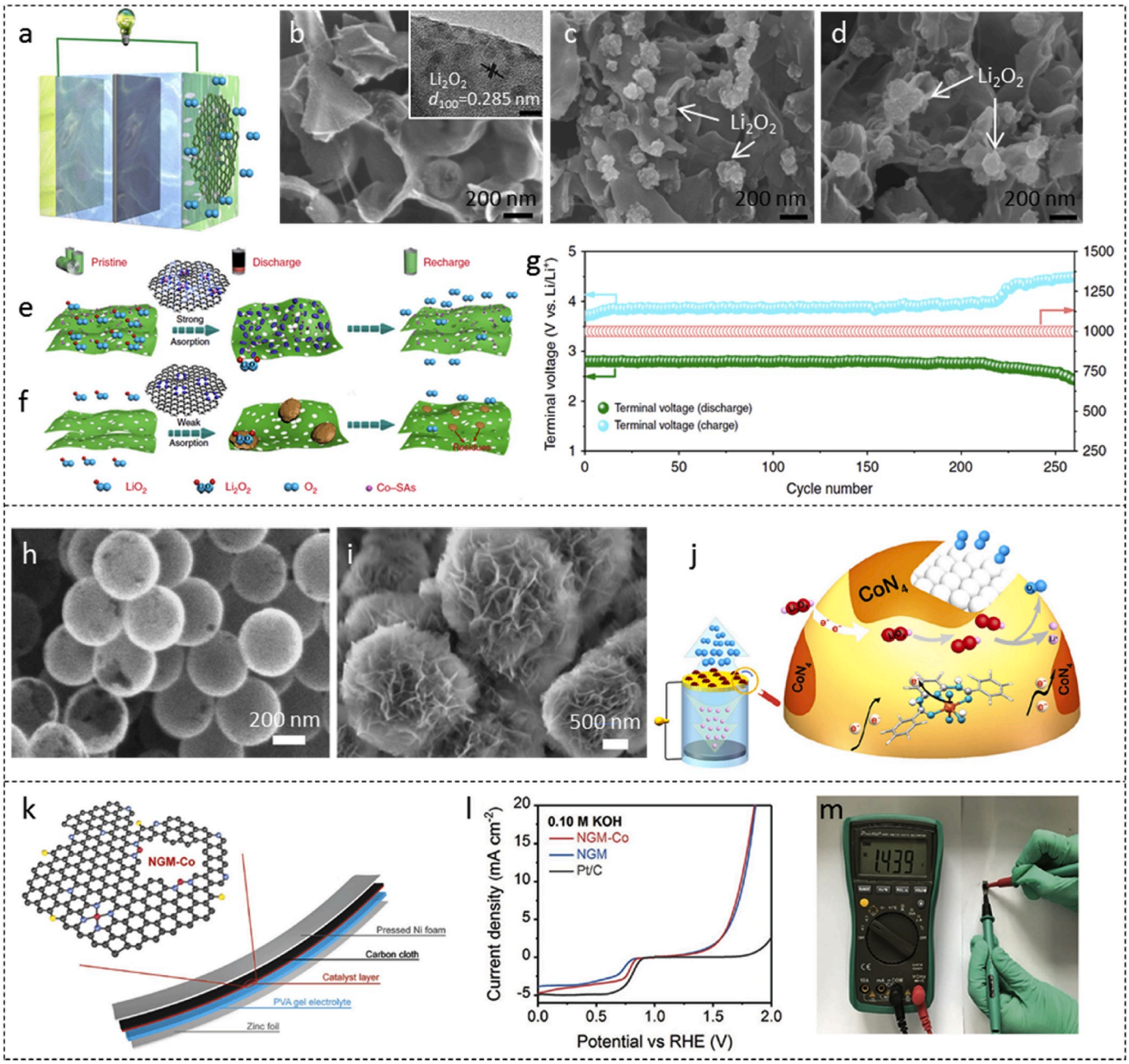

Fig. 6. a) Schematic of a Li–O_2 battery based on Co–SAs/N–C. b-d) Ex-situ scanning electron microscopy (SEM) images of b) Co–SAs/N–C, c) Co-NPs/N–C, and d) N–C electrode after the first charge cycle. Schematic illustration of the reaction mechanism taking place in e) Co–SAs/N–C and f) N–C electrodes, respectively. g) Cycling stability and terminal discharge–charge voltages of Co–SAs/N–C electrode for Li–O_2 battery. Reproduced with permission [29]. Copyright 2020, Nature Publishing Group. SEM images of h) N-HP-Co and i) N-HP-Co after discharge. j) Schematic illustration of the mechanisms of charging the N-HP-Co-catalyzed Li–O_2 batteries. Reproduced with permission [30]. Copyright 2020, Nature Publishing Group. k-m) NGM-Co for Zn-air batteries. k) Schematic illustration of the solid Zn-air battery. l) Linear sweep voltammetry curves of NGM-Co and control catalysts (10.0 mV s^{-1}), showing both the ORR and OER activity. m) Photograph of the Zn-air battery. Reproduced with permission [117]. Copyright 2017, Wiley-VCH.

Xu et al. prepared hollow N-doped carbon spheres with isolated single Co sites (NHP–Co) [30]. They found that, during the Li–O_2 battery discharge, atomic Co sites serve as nucleation sites for the growth of isolated nanosheet-like Li_2O_2 (Fig. 6h and i). During the subsequent charge, NHP–Co promote the decomposition of the Li_2O_2 by a one-electron pathway, which is kinetically more favorable and reversible compared to the two-electron pathway of commercial Pt/C (Fig. 6j). As a result, the Co–SAs-based Li–O_2 batteries showed an ultralong cycle life (261 cycles at a current density of 100 mA g^{-1} with a cut-off capacity of 1000 mAh g^{-1}) and a high discharge capacity (~14,777 mAh g^{-1} at a current density of 100 mA g^{-1}).

Regarding Zn-air batteries, the discharge-charge processes are also largely hindered by the sluggish reaction kinetics of ORR and OER at the air cathode. The conventional strategy to improve the reaction kinetics is to employ noble-metal-based catalysts, i.e., Pt-based catalysts for ORR and Ru/Ir-based catalysts for OER. However, the high cost and scarcity of these noble metals are inevitable problems for large scale commercialization. Recently, M-N-C has shown great promises for substituting precious-metal-based catalysts. Table 2 summarizes the performance of liquid and solid-state Zn-air batteries using ADMs as electrode materials. For example, Zhang et al. fabricated atomically dispersed Co-N_x-C active sites on graphene (NGM-Co) via defect engineering (Fig. 6k) [117]. As

Table 2
Summary of the properties of liquid and flexible solid-state Zn-air batteries by using ADMs as the cathode.

Sample on substrate	Feature	Loading amount (mg cm^{-2})	OCV (V)	Current density (mA cm^{-2} @ 1 V)	Peak power density (mW cm^{-2})	Ref.
S,N–Fe/N/C-CNT on carbon paper	liquid	1.25	1.35	~70	102.7	[51]
Co/N/O tri-doped graphene on carbon cloth	liquid	0.5	–	~75	152	[117]
Co/N/O tri-doped graphene on carbon cloth	solid-state	1.5	1.439	–	–	[117]
Fe–N-SCCFs on carbon fiber paper	liquid	1.0	–	205	297	[122]
NC-Co SA on carbon cloth	solid-state	1.35	1.411	~18	20.9	[123]
FeN_x-embedded PNC on carbon cloth	liquid	–	1.55	195	278	[124]
FeN_x-embedded PNC on carbon cloth	solid-state	–	1.436	59	118	[124]
(Fe,Co)/CNT on carbon fiber paper	liquid	1.0	1.63	178	260	[125]
Pd/MnO_2–CNT on carbon fiber paper	liquid	2.0	–	190.7	297.7	[126]
CoN_4/NG on carbon paper	liquid	1.0	1.51	~75	115	[127]
CoN_4/NG on carbon cloth	solid-state	1.5	–	~22	~28	[127]
Fe–SAs/NPS-HC on hydrophobic carbon paper	liquid	1.0	1.45	~100	195.0	[128]
Fe-N_x-C on Ni foam	liquid	–	1.51	~75	96.4	[118]
Fe-N_x-C on Ni foam	solid-state	–	1.493	–	–	[118]
SS-Co-SAC NSAs on carbon cloth	liquid	0.91	1.52	133.4	195.1	[129]
SS-Co-SAC NSAs on carbon cloth	solid-state	0.91	1.23	–	–	[129]
Co-POC on carbon cloth	liquid	0.1	–	~25	78	[130]
Zn/CoN–C on carbon paper	liquid	–	–	176	230	[121]
Zn–N–C-1 on carbon paper	liquid	0.5	–	~120	179	[119]
(Zn,Co)/NSC on carbon paper	liquid	1	1.5	~100	150	[120]
(Zn,Co)/NSC on carbon cloth	solid-state	5	1.56	~7	15	[120]
Cu ISAS/NC carbon fiber paper	liquid	1.0	–	~200	280	[71]
N and S co-doped Fe–N–C on Ni foam	liquid	1.0	1.53	~150	225.1	[131]

shown in Fig. 6l, this material displayed a superior bifunctional performance towards ORR/OER. The rechargeable solid Zn-air battery assembled using the NGM-Co-based air cathode was flexible and had a high open-circuit voltage (OCV) of 1.439 V (Fig. 6m), a small charge/-discharge voltage gap (0.7 V at 1.0 mA cm^{-2}), and high energy efficiency (63% at 1.0 mA cm^{-2}). Similarly, the Fe–N_x–C Zn-air battery had an OCV of 1.51 V and a power density of 96.4 mW cm^{-2} [118]. The rechargeable and foldable all-solid-state Zn-air based on the Fe-N_x-C catalyst had an OCV of 1.49 V and was able to function for 120 h. In another report, the use of Zn–N–C ADMs for Zn–O_2 batteries led to a maximum power density of 179 mW cm^{-2}, which is slightly higher than that obtained with Pt/C (173 mW cm^{-2}) [119].

In addition to the use of N and single-metal species, multi dopant and multi-metal sites have also been developed to improve the performance. Wu et al. achieved atomic dispersion of Fe-N_x species on N and S co-decorated hierarchical carbon layers (S,N–Fe/N/C-CNT) as a bifunctional OER/ORR catalyst [51]. Interestingly, S,N–Fe/N/C-CNT showed better OER/ORR activity than that of N–Fe/N/C-CNT. Such enhancement was probably attributed to the improved electrical conductivity of the material, resulting from the co-decoration N and S as well as the itinerant Fe 3d-electrons. The charge-discharge polarization curves of the S,N–Fe/N/C-CNT Zn-air battery showed an OCV of 1.35 V. Owing to the synergistic catalytic effects, dual metallic sites ADMs have also shown better OER/ORR activity than that of single-metal ADMs [120,121]. Zhang et al. synthesized atomically dispersed Zn and Co bimetallic catalyst supported on N and S co-doped carbon [120]. In this work, the S dopant was used to adjust the charge of the Zn, Co active centers and strengthen the interaction with oxygenated species. Moreover, the enhanced binding between O_2 and Zn–Co bimetallic sites facilitated the O–O activation and reduced the cleavage barrier of the O–O bond. This material had an outstanding ORR performance with a half-wave potential higher than that of commercial Pt/C (0.893 V vs. 0.826 V). A record-high voltage (1.56 V) was also achieved for the flexible solid-state Zn-air batteries based on this catalyst.

5. Understanding the role of SAs from an atomistic perspective

As outlined above, SAs, where isolated metal atoms are singly anchored on the support, are the ultimate limit for the downsizing metal particles or clusters. Reducing the metal particle size to isolated SAs can lead to i) a low coordination number of the metal centers due to unsaturated metal bonds [132,133]; ii) a discrete distribution of energy levels and a distinctive HOMO (highest occupied molecular orbital)-LUMO (lowest unoccupied molecular orbital) gap because of quantum confinement effects [134,135]; and iii) strong metal-support interactions, which are caused by the chemical bonding and charge transfer between metal SAs and supports [136]. As the particle size decreases, the surface Gibbs free energy increases and concomitantly, the metal becomes more active toward chemical interactions with both the support and the adsorbates [5]. Due to the quantum confinement, SAs exhibit unique chemical properties that are distinctly different from those of bulk metals, nanoparticles, or clusters. One should note that, if each SA functions as an active center, maximum atomic utilization can be achieved.

It is well known that, when the size reduces, quantum confinement effects are more pronounced. For example, quantum chemical calculations revealed that the electronic structure is highly dependent on the number of atoms present in an Au cluster [137]. Au atoms in small clusters ($n \leq 7$) have unsaturated coordination sites with a strongly localized electron density, as shown in Fig. 7. The more unsaturated coordination sites of the metal center are, the more active interactions between the metal sites and targeted molecules through the overlap of electronic orbitals will be [5,138]. Such a character has been employed to control Li plating in Li-metal batteries. In fact, where Li-ions preferentially nucleate near SA metal sites due to the much larger binding energy (0.5 eV) between Li and the SA decorated support compared to the pure substrate (0.1 eV) [32,95]. The easily formed Li_xM_y alloys can further guide the Li deposition with a much lower nucleation overpotential [32,95]. Thanks to their enhanced affinity between ADMs and

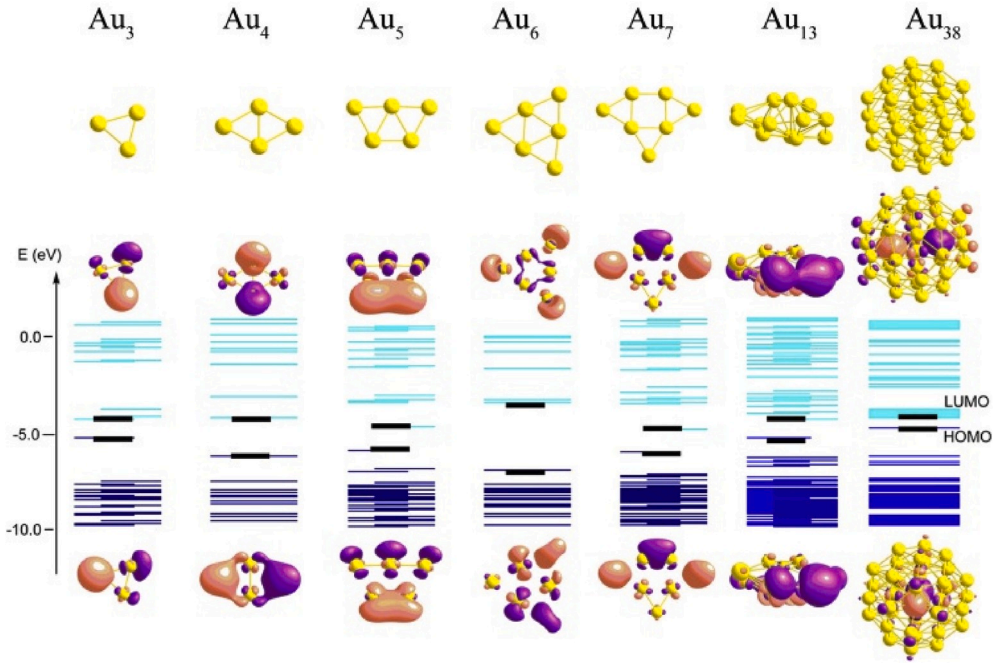

Fig. 7. The relationship between cluster size and the electronic structures by DFT calculations. Optimized structure (top), iso-surfaces of the LUMO (center) and HOMO (bottom) of the Au clusters. The energy levels are shown as horizontal lines. Reproduced with permission [137]. Copyright 2019, American Chemical Society.

Li-ions, Rosei and co-workers utilized a carbon cloth decorated with small clusters of Au atoms as a template to deposit Li and suppress the growth of dendrites [95]. In related work, Gong and co-authors investigated the use of SANi-NG as a Li host material to regulate the nucleation and deposition of Li experimentally and theoretically [10]. These authors further calculated that the binding energy of Li on SANi-NG (1.92 eV) is higher than that on pure graphene (1.23 eV), and even higher than that on Li itself (1.63 eV). This higher binding energy implies that Li atoms are more likely to nucleate on SANi-NG. The strong interactions between Li and ADMs were also observed in classical molecular dynamics (MD) simulations, in particular, Yan et al. found that Li atoms tend to accumulate near SA Fe-NG rather than pure carbon [96].

Since the coordination environment of SAs strongly depends on the metal and the support material, it is conceivable that different transition

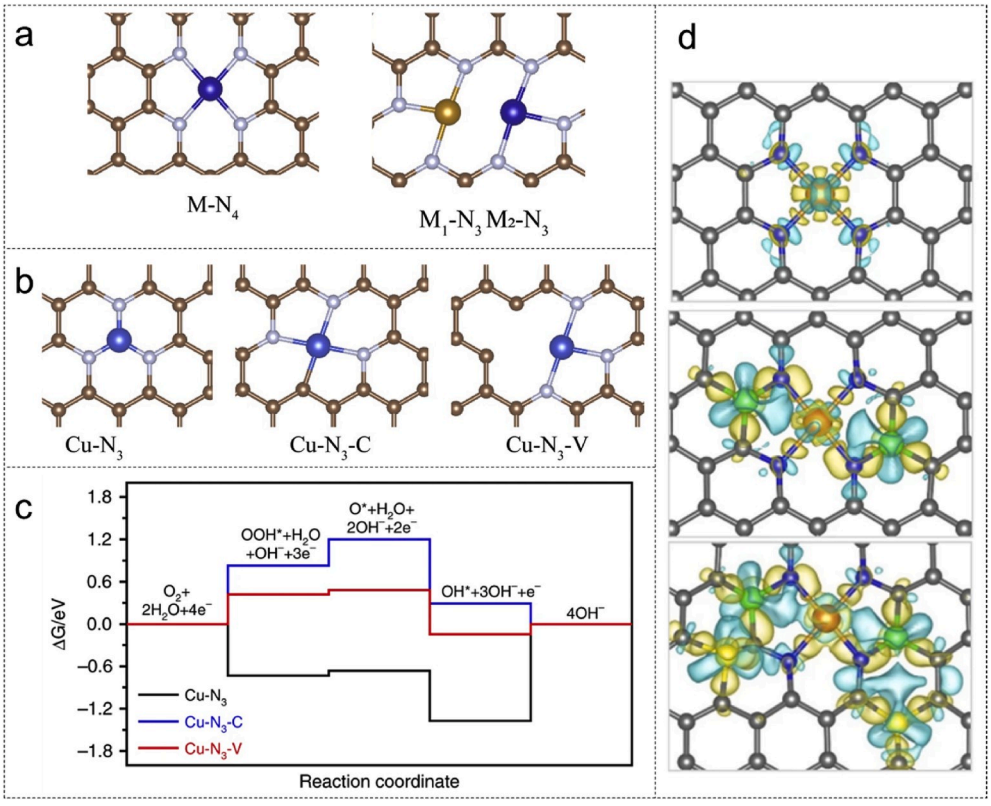

Fig. 8. a) Typical coordination structure of a single metal atom M, and dual metal atoms M_1 and M_2, supported on NG. Reproduced with permission [121]. Copyright 2019, Wiley Publishing Group. b) Different coordination structure models of a Cu SA on NG. c) Calculated reaction Gibbs free energy of the models grouped in panel (b). Reproduced with permission [71]. Copyright 2019, Nature Publishing Group. d) The calculated charge density differences of Fe SAs on different supports: top, single Fe on NG; middle, single Fe on P doped NG; bottom, single Fe on P, S co-doped NG. Yellow and blue areas represent charge density accumulation and loss, respectively. Reproduced with permission [128]. Copyright 2019, Nature Publishing Group.

metals SAs supported on graphene or NG may share similar coordination patterns [139]. Both experimental characterizations and theoretical calculations confirmed that metal atoms coordinated with 3 or 4 N atoms to form Fe–N_4 [51,128], Co–N_4 [123], Zn–N_4 [119], Cu–N_3 [71], Zn–N_3–Co–N_3 [121], or Fe–N_3–Co–N_3 [125] are substantially more stable, see Fig. 8a. For GO, one single Fe atom coordinates with 4 O atoms to form the Fe–O_4 motif [83]. It has been argued that the 4 coordinated O atoms are essential to haul Fe out of the bulk crystal and impede its agglomeration on the GO surface [83]. The electrochemical performance is also dependent on the bonding of the SAs. For instance, first-principle calculations suggest that the Cu–N_3's (Fig. 8b left) ORR rate-determining step is the OH* removal reaction, conversely, the formation of OOH* is rate-determining if one vacant site is present, i.e., for the Cu–N_3–V structure, see Fig. 8b right [71]. Additionally, the computed overpotential depends on the Cu coordination where Cu–N_3–V performs better towards ORR (overpotential = 0.52 V) compared to Cu–N_3 (1.37 V) or Cu–N_3–C (0.83 V), see Fig. 8c [71]. The much lower overpotential was attributed to the introduction of the vacancies that triggered a non-symmetric redistribution of electrons around the Cu atoms.

The specific SAs and supports chosen may have a significant impact on the electronic structure hence strongly influence the catalytic activity. For example, the chemical potential difference between the SA metal and the support material may lead to a redistribution of the electron density around the metal sites. As a result, the anchored metal atoms are usually positively charged [5]. Li and co-workers calculated the electron density of a single Fe on the N, P, and S co-doped hollow carbon (NPS-HC). Their study revealed that the Fe atom attracted more electrons from the neighboring S and P atoms compared to N doped HC and N, P co-doped HC (Fig. 8d), making Fe less positively charged [128]. Accordingly, the single Fe supported on NPS-HC was predicted to be the best ORR catalyst among the materials studied, where its superior performance was confirmed experimentally.

Atomistic calculations, like DFT and MD simulations, have helped to understand the mechanism underpinning the enhanced performance following the introduction of SAs or clusters. Zhou et al. searched computationally for the best SA supported on NG for Li–S batteries [140]. These authors calculated that, for SA metals on NG as the support, LiPSs have larger energies of adsorption (up to 2–3 eV for Li_2S_6) and the decomposition of Li_2S is characterized by a smaller barrier (~1 eV), compared to the pure graphene or nitrogen-doped graphene sheets [140]. The small barrier for the decomposition of Li_2S was attributed to the weakening of the Li–S bond caused by the electron transfer between the S and the metal centers [140]. As a guideline suggested by Cui et al. for Li–S battery design [141], catalysts with a low Li_2S decomposition barrier and a strong interaction with LiPSs are needed because i) decreasing the decomposition barrier of Li_2S can increase the utilization of active materials thereby decreasing the formation of dead Li_2S, and ii) the stronger chemical interaction with LiPSs can effectively suppress the shuttle effect [141]. Among all the investigated cases, V SAs, which were computed to have the largest binding energy of Li_2S_6 (3.38 eV) and the lowest Li_2S decomposition barrier (1.10 eV), are expected to be preferential to reach the above goals. We must note that, for comparison, the adsorption energy of Li_2S_6 and the decomposition barrier of Li_2S on pure graphene is only 0.76 eV and 2.12 eV, respectively. The theoretical investigations were followed by experiments where V SAs were found to be able to improve the high-rate performance and endow a long-life in Li–S batteries (a capacity of 645 mAh g^{-1} at 3 C and a capacity decay of 0.073% per cycle over 400 cycles was achieved). Chou and co-workers used DFT and *ab initio* MD to reveal the adsorption behavior of NaPSs for a Co_6 cluster supported on sp^3 carbon, which consisted of 216 carbon atoms and two exposed surfaces [34]. It was predicted that the presence of the Co_6 cluster spontaneously decomposes the Na_2S_4 molecule to Na_2S_2 and Na_2S. Such a fast reduction of Na_2S_4 was attributed to the facile formation of Co–S bonds.

The low-coordination environment of ADMs coupled with the enhanced interactions with the support, can provide an excellent catalytic performance in a variety of heterogeneous reactions, such as ORR, OER, HER. Consequently, ADMs have been extensively employed as active catalysts in Zn-air or Li–O_2 batteries. DFT calculations have also been utilized to understand the mechanism underpinning the improved performance. Xu and co-authors investigated the use of the Co SAs as a cathode catalyst for the decomposition of Li_2O_2, one of the most critical steps for the kinetics of ORR/OER in the Li–O_2 batteries [30]. They observed that the synergy between the Co SAs and the support effectively lowers the binding energy (−1.03 eV) of the LiO_2, the reduced species of Li_2O_2, on the cathode materials in the presence of Co SAs. As a comparison, the binding energy of LiO_2 without the Co SA is more negative (−1.85 eV). The weaker interaction between the reduced species of Li_2O_2 (LiO_2 ion pairs) and the cathode thus promoted the decomposition of Li_2O_2 following the one-electron reaction. In another work, Yin and co-workers studied Co–SAs/N–C as a dual catalyst for Li–O_2 batteries [29]. There, they observed that the cobalt-nitrogen moieties tuned the evolution mechanism of Li_2O_2 to follow the one-electron pathway as well. For Zn-air batteries, a variety of materials decorated with isolated atoms or clusters have been exploited. Wu et al. studied the Cu SAs as a cathode catalyst for ORR in Zn-air batteries and explained that the improved performance is due to the significantly lower overpotential enabled by Cu–N_3–V [71], see Fig. 8b and c. Chu and co-workers designed a new bifunctional ORR/OER catalyst with atomically dispersed Fe-N_x species on N and S co-doped hierarchical carbon layers [51]. Theoretical calculations also confirmed that the developed catalyst shows much lower overpotential (0.24 V) in the alkaline condition, enabling a maximum power density of Zn-air battery as high as 102.7 mW cm^{-2}. Sun and co-workers investigated the ORR mechanism for Zn–Co pairs coordinated on NG [121]. They demonstrated that the structural motif with bonded Zn and Co, as shown in the bottom of Fig. 8a, has the lowest energy compared to those of non-bonded Zn–Co atoms, highlighting the advantages of forming Co–Zn diatomic pairs, which can facilitate the O_2 decomposition by elongating the O═O bond. Similar findings have also been documented in a study of Fe–Co dual sites [125].

6. Summary and outlook

Thanks to the unsaturated coordination configuration of active centers, quantum confinement effects, and the synergy with the support, ADMs exhibit catalytic activity and selectivity much higher than their nanoparticle and bulk counterparts. As outlined above in Section 2, one of the biggest challenges is still to prepare well defined ADMs. It is worth noting that: i) the synthesis of ADMs involves processes ranging from ultralow (−40 °C) to high (1000 °C) temperatures; ii) SAs can be formed using strategies involving different states, including gas, liquid, and solid; and iii) external factors, including heat, electromagnetic, and mechanical interactions, can facilitate the formation of defects on the supports as well as favor the chemical bonds between the support and the SA metals; iv) highly defective supports with abundant micropores, vacancies, and heteroatomic dopants (e.g. N, O, S, and C) can enable the confinement and bonding of SAs. These controllable strategies provide many effective approaches for designing ADMs with strong metal-support interactions and high SA loadings. Thanks to the high electrocatalytic activity towards electrochemical processes such as LiPS conversion in Li–S/Na–S batteries and OER/ORR in Li–O_2 and Zn-air batteries, ADMs are among the most promising materials for several energy storage applications. In addition, ADMs with an ultra-high dispersion of metal sites increase the density of Li nucleation sites for Li plating/stripping, leading to the formation of dendrite-free Li anodes and thus drastically improving the performance of Li metal batteries.

Although significant progress has been achieved so far, considerable challenges remain especially for the employment of ADMs in commercial energy storage devices. We must state that challenges also imply ample opportunities to expand the field. Future research might be

devoted to the following:

i. Developing scalable, cost-effective, and facile methods with high-loading SAs without sacrificing the stability to propel the commercialization of ADMs. Most ADMs have been achieved only at a laboratory scale and there is a long way to large scale production. Facile synthetic methods involving low-cost raw materials, more affordable equipment, less sophisticated protocols, and milder reaction conditions should be developed. Another critical problem is the SA loading. The SA loadings in most literature are very low, where a significant amount of metal atoms are wasted during the synthesis, thus making SA catalysts not that atomically economic as expected. However, high SA loadings inevitably cause aggregations, hence, maintaining the subtle balance between loading and stability must be considered as well. From the above, it is apparent that the most challenging problem in this field is still the preparation.
ii. Designing new kinds of ADMs by tuning the active sites and/or support environments. ADMs have limited ability to catalyze certain reactions (e.g. the alcohol oxidation reaction) due to their sole and/or low-density active sites [142]. In this regard, multi-metallic atoms (e.g. dual-metal dimers) or highly dense SAs would activate more electrochemical reactions by introducing the synergistic effect. For instance, multi-metal SAs might be particularly desirable to catalyze multiple reactions involved in one energy storage device. Besides, the coordination environment of SAs is also important. SAs with different binding environments could lead to different electrochemical activities.
iii. Studying the mechanism underpinning the synthesis of ADMs and their applications. Some ADMs can be obtained in technique, but in which the formation mechanism is still unclear. For instance, some methods that are suitable for the construction of noble-metal ADMs are not applicable to non-noble-metal ones and vice versa. In this regard, in situ/operando studies will play an essential role in unveiling the mechanism. As for the applications of ADMs, the direct analysis of SAs during reactions would also reveal the specifics of the structure-performance relationships and elucidate the reaction mechanisms as well. These studies are urgently needed to design SA-based materials rationally.
iv. Understanding the SAs impacts during the catalyzing reactions using the atomistic calculations and other computation techniques. Undoubtedly, theoretical calculations can continue to guide the design of new SAs with the desired energy storage performance in many aspects, such as binding environment simulation, free Gibbs energy calculation, reaction performance prediction, mechanistic study, establishing the fundamental structure/property correlation and so on.
v. Reducing the activity loss of SAs. SAs may aggregate into clusters or even nanoparticles over time, resulting in irreversible loss of activity. In addition, SAs may leach as a result of the substrate corrosion. A basic strategy for reducing the activity loss is to improve the metal-support interaction by physical confinement and chemical bonding of SAs. Conversely, the support needs to be stable chemically and structurally.
vi. Extending the applications of ADMs to other energy storage devices. It is expected that ADMs could exhibit enhanced performance when employed for other energy storage devices, such as potassium-based, Zn–CO_2, and Li–CO_2 batteries. For instance, ADMs favor the electrochemical reduction of CO_2, which is also an essential process involved in metal-CO_2 batteries. In this case, ADMs could facilitate the charge/discharge process via catalytic action. In addition, RuO_2 is used in commercial capacitors. Consequently, the SAs of Ru supported on porous carbon are expected to show an enhanced super capacitive performance.

In conclusion, ADMs have shown great potential in resolving the challenges faced by electrochemical energy storage systems. It should be noted that the development of ADMs is still in its infancy. Consequently, more experimental and theoretical efforts regarding SAs may result in boosting the performance of many energy storage devices. Many more breakthroughs can be envisioned in this rapidly booming field.

Declaration of competing interest

The authors declare that they have no known competing financial interests or personal relationships that could have appeared to influence the work reported in this paper.

Acknowledgements

This work was jointly supported by the Research Grants Council of Hong Kong (GRF Projects: 16207615 and 16204517), the Guangzhou Science and Technology Program (No. 201807010074), Hong Kong Innovation and Technology Fund (No. ITS/292/18FP) and the Science and Technology Planning Project of Guangdong Province, China (2017A050506014). A. Curcio kindly recognizes the support of the Hong Kong Ph.D. Fellowship Scheme.

References

[1] Z.W. Seh, J. Kibsgaard, C.F. Dickens, I. Chorkendorff, J.K. Nørskov, T. F. Jaramillo, Science 355 (2017), eaad4998.
[2] S. Chu, Y. Cui, N. Liu, Nat. Mater. 16 (2017) 16–22.
[3] Q. Zhang, E. Uchaker, S.L. Candelaria, G. Cao, Chem. Soc. Rev. 42 (2013) 3127–3171.
[4] B. Qiao, A. Wang, X. Yang, L.F. Allard, Z. Jiang, Y. Cui, J. Liu, J. Li, T. Zhang, Nat. Chem. 3 (2011) 634–641.
[5] X.-F. Yang, A. Wang, B. Qiao, J. Li, J. Liu, T. Zhang, Acc. Chem. Res. 46 (2013) 1740–1748.
[6] H. Zhang, G. Liu, L. Shi, J. Ye, Adv. Energy Mater. 8 (2018) 1701343.
[7] Z. Zhang, Y. Chen, L. Zhou, C. Chen, Z. Han, B. Zhang, Q. Wu, L. Yang, L. Du, Y. Bu, P. Wang, X. Wang, H. Yang, Z. Hu, Nat. Commun. 10 (2019) 1657.
[8] S. Yang, J. Kim, Y.J. Tak, A. Soon, H. Lee, Angew. Chem. Int. Ed. 55 (2016) 2058–2062.
[9] G. Kyriakou, M.B. Boucher, A.D. Jewell, E.A. Lewis, T.J. Lawton, A.E. Baber, H. L. Tierney, M. Flytzani Stephanopoulos, E.C.H. Sykes, Science 335 (2012) 1209–1212.
[10] X. Li, W. Bi, L. Zhang, S. Tao, W. Chu, Q. Zhang, Y. Luo, C. Wu, Y. Xie, Adv. Mater. 28 (2016) 2427–2431.
[11] S.K. Sahoo, Y. Ye, S. Lee, J. Park, H. Lee, J. Lee, J.W. Han, ACS Energy Lett 4 (2019) 126–132.
[12] H. Li, L. Wang, Y. Dai, Z. Pu, Z. Lao, Y. Chen, M. Wang, X. Zheng, J. Zhu, W. Zhang, R. Si, C. Ma, J. Zeng, Nat. Nanotechnol. 13 (2018) 411–417.
[13] J. Zhang, X. Wu, W.-C. Cheong, W. Chen, R. Lin, J. Li, L. Zheng, W. Yan, L. Gu, C. Chen, Q. Peng, D. Wang, Y. Li, Nat. Commun. 9 (2018) 1002.
[14] J. Yan, L. Kong, Y. Ji, J. White, Y. Li, J. Zhang, P. An, S. Liu, S.-T. Lee, T. Ma, Nat. Commun. 10 (2019) 2149.
[15] M. Fan, J.D. Jimenez, S.N. Shirodkar, J. Wu, S. Chen, L. Song, M.M. Royko, J. Zhang, H. Guo, J. Cui, K. Zuo, W. Wang, C. Zhang, F. Yuan, R. Vajtai, J. Qian, J. Yang, B.I. Yakobson, J.M. Tour, J. Lauterbach, D. Sun, P.M. Ajayan, ACS Catal. 9 (2019) 10077–10086.
[16] L. Wang, X. Duan, X. Liu, J. Gu, R. Si, Y. Qiu, Y. Qiu, D. Shi, F. Chen, X. Sun, J. Lin, J. Sun, Adv. Energy Mater. 10 (2020) 1903137.
[17] S. Li, J. Liu, Z. Yin, P. Ren, L. Lin, Y. Gong, C. Yang, X. Zheng, R. Cao, S. Yao, Y. Deng, X. Liu, L. Gu, W. Zhou, J. Zhu, X. Wen, B. Xu, D. Ma, ACS Catal. 10 (2020) 907–913.
[18] Y. Chen, S. Ji, C. Chen, Q. Peng, D. Wang, Y. Li, Joule 2 (2018) 1242–1264.
[19] J. Lin, A. Wang, B. Qiao, X. Liu, X. Yang, X. Wang, J. Liang, J. Li, J. Liu, T. Zhang, J. Am. Chem. Soc. 135 (2013) 15314–15317.
[20] H. Wei, X. Liu, A. Wang, L. Zhang, B. Qiao, X. Yang, Y. Huang, S. Miao, J. Liu, T. Zhang, Nat. Commun. 5 (2014) 5634.
[21] Z. Zhang, Y. Zhu, H. Asakura, B. Zhang, J. Zhang, M. Zhou, Y. Han, T. Tanaka, A. Wang, T. Zhang, N. Yan, Nat. Commun. 8 (2017) 16100.
[22] G. Vilé, D. Albani, M. Nachtegaal, Z. Chen, D. Dontsova, M. Antonietti, N. López, J. Pérez-Ramírez, Angew. Chem. Int. Ed. 54 (2015) 11265–11269.
[23] H. Fei, J. Dong, D. Chen, T. Hu, X. Duan, I. Shakir, Y. Huang, X. Duan, Chem. Soc. Rev. 48 (2019) 5207–5241.
[24] T. Wang, Q. Zhao, Y. Fu, C. Lei, B. Yang, Z. Li, L. Lei, G. Wu, Y. Hou, Small Methods 3 (2019) 1900210.
[25] L. Zhang, Y. Wang, Z. Niu, J. Chen, Small Methods 3 (2019) 1800443.
[26] M. Liu, L. Wang, K. Zhao, S. Shi, Q. Shao, L. Zhang, X. Sun, Y. Zhao, J. Zhang, Energy Environ. Sci. 12 (2019) 2890–2923.
[27] Y. Song, W. Cai, L. Kong, J. Cai, Q. Zhang, J. Sun, Adv. Energy Mater. 10 (2020) 1901075.

[28] L. Du, Q. Wu, L. Yang, X. Wang, R. Che, Z. Lyu, W. Chen, X. Wang, Z. Hu, Nano Energy 57 (2019) 34–40.
[29] P. Wang, Y. Ren, R. Wang, P. Zhang, M. Ding, C. Li, D. Zhao, Z. Qian, Z. Zhang, L. Zhang, L. Yin, Nat. Commun. 11 (2020) 1576.
[30] L.-N. Song, W. Zhang, Y. Wang, X. Ge, L.-C. Zou, H.-F. Wang, X.-X. Wang, Q.-C. Liu, F. Li, J.-J. Xu, Nat. Commun. 11 (2020) 2191.
[31] Q. Liu, Y. Wang, L. Dai, J. Yao, Adv. Mater. 28 (2016) 3000–3006.
[32] P. Zhai, T. Wang, W. Yang, S. Cui, P. Zhang, A. Nie, Q. Zhang, Y. Gong, Adv. Energy Mater. 9 (2019) 1804019.
[33] J. Xie, B.-Q. Li, H.-J. Peng, Y.-W. Song, M. Zhao, X. Chen, Q. Zhang, J.-Q. Huang, Adv. Mater. 31 (2019) 1903813.
[34] B.-W. Zhang, T. Sheng, Y.-D. Liu, Y.-X. Wang, L. Zhang, W.-H. Lai, L. Wang, J. Yang, Q.-F. Gu, S.-L. Chou, H.-K. Liu, S.-X. Dou, Nat. Commun. 9 (2018) 4082.
[35] J. Liu, M. Jiao, L. Lu, H.M. Barkholtz, Y. Li, Y. Wang, L. Jiang, Z. Wu, D.-j. Liu, L. Zhuang, C. Ma, J. Zeng, B. Zhang, D. Su, P. Song, W. Xing, W. Xu, Y. Wang, Z. Jiang, G. Sun, Nat. Commun. 8 (2017) 15938.
[36] C. Zhang, J. Sha, H. Fei, M. Liu, S. Yazdi, J. Zhang, Q. Zhong, X. Zou, N. Zhao, H. Yu, Z. Jiang, E. Ringe, B.I. Yakobson, J. Dong, D. Chen, J.M. Tour, ACS Nano 11 (2017) 6930–6941.
[37] J. Zhang, Y. Zhao, C. Chen, Y.-C. Huang, C.-L. Dong, C.-J. Chen, R.-S. Liu, C. Wang, K. Yan, Y. Li, G. Wang, J. Am. Chem. Soc. 141 (2019) 20118–20126.
[38] Y. Zhu, W. Sun, J. Luo, W. Chen, T. Cao, L. Zheng, J. Dong, J. Zhang, M. Zhang, Y. Han, C. Chen, Q. Peng, D. Wang, Y. Li, Nat. Commun. 9 (2018) 3861.
[39] X. Rong, H.-J. Wang, X.-L. Lu, R. Si, T.-B. Lu, Angew. Chem. Int. Ed. 59 (2020) 1961–1965.
[40] L. Zhang, D. Liu, Z. Muhammad, F. Wan, W. Xie, Y. Wang, L. Song, Z. Niu, J. Chen, Adv. Mater. 31 (2019) 1903955.
[41] P. Song, M. Luo, X. Liu, W. Xing, W. Xu, Z. Jiang, L. Gu, Adv. Funct. Mater. 27 (2017) 1700802.
[42] W. Chen, J. Pei, C.-T. He, J. Wan, H. Ren, Y. Zhu, Y. Wang, J. Dong, S. Tian, W.-C. Cheong, S. Lu, L. Zheng, X. Zheng, W. Yan, Z. Zhuang, C. Chen, Q. Peng, D. Wang, Y. Li, Angew. Chem. Int. Ed. 56 (2017) 16086–16090.
[43] P. Yin, T. Yao, Y. Wu, L. Zheng, Y. Lin, W. Liu, H. Ju, J. Zhu, X. Hong, Z. Deng, G. Zhou, S. Wei, Y. Li, Angew. Chem. Int. Ed. 55 (2016) 10800–10805.
[44] X. Wang, W. Chen, L. Zhang, T. Yao, W. Liu, Y. Lin, H. Ju, J. Dong, L. Zheng, W. Yan, X. Zheng, Z. Li, X. Wang, J. Yang, D. He, Y. Wang, Z. Deng, Y. Wu, Y. Li, J. Am. Chem. Soc. 139 (2017) 9419–9422.
[45] X.X. Wang, D.A. Cullen, Y.-T. Pan, S. Hwang, M. Wang, Z. Feng, J. Wang, M. H. Engelhard, H. Zhang, Y. He, Y. Shao, D. Su, K.L. More, J.S. Spendelow, G. Wu, Adv. Mater. 30 (2018) 1706758.
[46] H. Zhang, S. Hwang, M. Wang, Z. Feng, S. Karakalos, L. Luo, Z. Qiao, X. Xie, C. Wang, D. Su, Y. Shao, G. Wu, J. Am. Chem. Soc. 139 (2017) 14143–14149.
[47] Y. Chen, S. Ji, Y. Wang, J. Dong, W. Chen, Z. Li, R. Shen, L. Zheng, Z. Zhuang, D. Wang, Y. Li, Angew. Chem. Int. Ed. 56 (2017) 6937–6941.
[48] H. Fei, J. Dong, M.J. Arellano-Jiménez, G. Ye, N. Dong Kim, E.L.G. Samuel, Z. Peng, Z. Zhu, F. Qin, J. Bao, M.J. Yacaman, P.M. Ajayan, D. Chen, J.M. Tour, Nat. Commun. 6 (2015) 8668.
[49] H. Fei, J. Dong, Y. Feng, C.S. Allen, C. Wan, B. Volosskiy, M. Li, Z. Zhao, Y. Wang, H. Sun, P. An, W. Chen, Z. Guo, C. Lee, D. Chen, I. Shakir, M. Liu, T. Hu, Y. Li, A. I. Kirkland, X. Duan, Y. Huang, Nat. Catal. 1 (2018) 63–72.
[50] L. Zhang, Y. Jia, G. Gao, X. Yan, N. Chen, J. Chen, M.T. Soo, B. Wood, D. Yang, A. Du, X. Yao, Inside Chem. 4 (2018) 285–297.
[51] P. Chen, T. Zhou, L. Xing, K. Xu, Y. Tong, H. Xie, L. Zhang, W. Yan, W. Chu, C. Wu, Y. Xie, Angew. Chem. Int. Ed. 56 (2017) 610–614.
[52] M. Zhang, Y.-G. Wang, W. Chen, J. Dong, L. Zheng, J. Luo, J. Wan, S. Tian, W.-C. Cheong, D. Wang, Y. Li, J. Am. Chem. Soc. 139 (2017) 10976–10979.
[53] H. Zhang, P. An, W. Zhou, B.Y. Guan, P. Zhang, J. Dong, X.W. Lou, Sci. Adv. 4 (2018), eaao6657.
[54] L. Zhao, Y. Zhang, L.-B. Huang, X.-Z. Liu, Q.-H. Zhang, C. He, Z.-Y. Wu, L.-J. Zhang, J. Wu, W. Yang, L. Gu, J.-S. Hu, L.-J. Wan, Nat. Commun. 10 (2019) 1278.
[55] Y. Zhu, W. Sun, W. Chen, T. Cao, Y. Xiong, J. Luo, J. Dong, L. Zheng, J. Zhang, X. Wang, C. Chen, Q. Peng, D. Wang, Y. Li, Adv. Funct. Mater. 28 (2018) 1802167.
[56] P. Liu, Y. Zhao, R. Qin, S. Mo, G. Chen, L. Gu, D.M. Chevrier, P. Zhang, Q. Guo, D. Zang, B. Wu, G. Fu, N. Zheng, Science 352 (2016) 797–800.
[57] H. Wei, K. Huang, D. Wang, R. Zhang, B. Ge, J. Ma, B. Wen, S. Zhang, Q. Li, M. Lei, C. Zhang, J. Irawan, L.-M. Liu, H. Wu, Nat. Commun. 8 (2017) 1490.
[58] H. Wei, H. Wu, K. Huang, B. Ge, J. Ma, J. Lang, D. Zu, M. Lei, Y. Yao, W. Guo, H. Wu, Chem. Sci. 10 (2019) 2830–2836.
[59] J. Ji, Y. Zhang, L. Tang, C. Liu, X. Gao, M. Sun, J. Zheng, M. Ling, C. Liang, Z. Lin, Nano Energy 63 (2019) 103849.
[60] X. Li, J. Yu, J. Jia, A. Wang, L. Zhao, T. Xiong, H. Liu, W. Zhou, Nano Energy 62 (2019) 127–135.
[61] T. Li, J. Liu, Y. Song, F. Wang, ACS Catal. 8 (2018) 8450–8458.
[62] G. Dong, M. Fang, H. Wang, S. Yip, H.-Y. Cheung, F. Wang, C.-Y. Wong, S.T. Chu, J.C. Ho, J. Mater. Chem. A 3 (2015) 13080–13086.
[63] M. Tavakkoli, N. Holmberg, R. Kronberg, H. Jiang, J. Sainio, E.I. Kauppinen, T. Kallio, K. Laasonen, ACS Catal. 7 (2017) 3121–3130.
[64] L. Zhang, L. Han, H. Liu, X. Liu, J. Luo, Angew. Chem. Int. Ed. 56 (2017) 13694–13698.
[65] J. Zhang, Y. Zhao, X. Guo, C. Chen, C.-L. Dong, R.-S. Liu, C.-P. Han, Y. Li, Y. Gogotsi, G. Wang, Nat. Catal. 1 (2018) 985–992.
[66] Y. Xue, B. Huang, Y. Yi, Y. Guo, Z. Zuo, Y. Li, Z. Jia, H. Liu, Y. Li, Nat. Commun. 9 (2018) 1460.
[67] N. Cheng, S. Stambula, D. Wang, M.N. Banis, J. Liu, A. Riese, B. Xiao, R. Li, T.-K. Sham, L.-M. Liu, G.A. Botton, X. Sun, Nat. Commun. 7 (2016) 13638.
[68] H. Yan, H. Cheng, H. Yi, Y. Lin, T. Yao, C. Wang, J. Li, S. Wei, J. Lu, J. Am. Chem. Soc. 137 (2015) 10484–10487.
[69] H. Yan, Y. Lin, H. Wu, W. Zhang, Z. Sun, H. Cheng, W. Liu, C. Wang, J. Li, X. Huang, T. Yao, J. Yang, S. Wei, J. Lu, Nat. Commun. 8 (2017) 1070.
[70] Y. Qu, Z. Li, W. Chen, Y. Lin, T. Yuan, Z. Yang, C. Zhao, J. Wang, C. Zhao, X. Wang, F. Zhou, Z. Zhuang, Y. Wu, Y. Li, Nat. Catal. 1 (2018) 781–786.
[71] Z. Yang, B. Chen, W. Chen, Y. Qu, F. Zhou, C. Zhao, Q. Xu, Q. Zhang, X. Duan, Y. Wu, Nat. Commun. 10 (2019) 3734.
[72] Y. Qu, B. Chen, Z. Li, X. Duan, L. Wang, Y. Lin, T. Yuan, F. Zhou, Y. Hu, Z. Yang, C. Zhao, J. Wang, C. Zhao, Y. Hu, G. Wu, Q. Zhang, Q. Xu, B. Liu, P. Gao, R. You, W. Huang, L. Zheng, L. Gu, Y. Wu, Y. Li, J. Am. Chem. Soc. 141 (2019) 4505–4509.
[73] T. He, S. Chen, B. Ni, Y. Gong, Z. Wu, L. Song, L. Gu, W. Hu, X. Wang, Angew. Chem. Int. Ed. 57 (2018) 3493–3498.
[74] M. Gauthier, D. Mazouzi, D. Reyter, B. Lestriez, P. Moreau, D. Guyomard, L. Roué, Energy Environ. Sci. 6 (2013) 2145–2155.
[75] S. Immohr, M. Felderhoff, C. Weidenthaler, F. Schüth, Angew. Chem. Int. Ed. 52 (2013) 12688–12691.
[76] Z. Liu, X. Chang, T. Wang, W. Li, H. Ju, X. Zheng, X. Wu, C. Wang, J. Zheng, X. Li, ACS Nano 11 (2017) 6065–6073.
[77] D. Deng, X. Chen, L. Yu, X. Wu, Q. Liu, Y. Liu, H. Yang, H. Tian, Y. Hu, P. Du, R. Si, J. Wang, X. Cui, H. Li, J. Xiao, T. Xu, J. Deng, F. Yang, P.N. Duchesne, P. Zhang, J. Zhou, L. Sun, J. Li, X. Pan, X. Bao, Sci. Adv. 1 (2015), e1500462.
[78] X. Cui, J. Xiao, Y. Wu, P. Du, R. Si, H. Yang, H. Tian, J. Li, W.-H. Zhang, D. Deng, X. Bao, Angew. Chem. Int. Ed. 55 (2016) 6708–6712.
[79] X. Chen, L. Yu, S. Wang, D. Deng, X. Bao, Nano Energy 32 (2017) 353–358.
[80] X. Cui, H. Li, Y. Wang, Y. Hu, L. Hua, H. Li, X. Han, Q. Liu, F. Yang, L. He, X. Chen, Q. Li, J. Xiao, D. Deng, X. Bao, Inside Chem. 4 (2018) 1902–1910.
[81] Y. Yao, Z. Huang, P. Xie, L. Wu, L. Ma, T. Li, Z. Pang, M. Jiao, Z. Liang, J. Gao, Y. He, D.J. Kline, M.R. Zachariah, C. Wang, J. Lu, T. Wu, T. Li, C. Wang, R. Shahbazian-Yassar, L. Hu, Nat. Nanotechnol. 14 (2019) 851–857.
[82] T.H.M. Lau, S. Wu, R. Kato, T.-S. Wu, J. Kulhavý, J. Mo, J. Zheng, J.S. Foord, Y.-L. Soo, K. Suenaga, M.T. Darby, S.C.E. Tsang, ACS Catal. 9 (2019) 7527–7534.
[83] Y. Qu, L. Wang, Z. Li, P. Li, Q. Zhang, Y. Lin, F. Zhou, H. Wang, Z. Yang, Y. Hu, M. Zhu, X. Zhao, X. Han, C. Wang, Q. Xu, L. Gu, J. Luo, L. Zheng, Y. Wu, Adv. Mater. 31 (2019) 1904496.
[84] Z. Zhang, Q. Wu, K. Mao, Y. Chen, L. Du, Y. Bu, O. Zhuo, L. Yang, X. Wang, Z. Hu, ACS Catal. 8 (2018) 8477–8483.
[85] B. Yue, Y. Ma, H. Tao, L. Yu, G. Jian, X. Wang, X. Wang, Y. Lu, Z. Hu, J. Mater. Chem. 18 (2008) 1747–1750.
[86] H. Fei, J. Dong, C. Wan, Z. Zhao, X. Xu, Z. Lin, Y. Wang, H. Liu, K. Zang, J. Luo, S. Zhao, W. Hu, W. Yan, I. Shakir, Y. Huang, X. Duan, Adv. Mater. 30 (2018) 1802146.
[87] Y. Zhu, J. Sokolowski, X. Song, Y. He, Y. Mei, G. Wu, Adv. Energy Mater. 10 (2020) 1902844.
[88] W. Xu, J. Wang, F. Ding, X. Chen, E. Nasybulin, Y. Zhang, J.-G. Zhang, Energy Environ. Sci. 7 (2014) 513–537.
[89] P.G. Bruce, S.A. Freunberger, L.J. Hardwick, J.-M. Tarascon, Nat. Mater. 11 (2012) 19–29.
[90] Z. Peng, S.A. Freunberger, Y. Chen, P.G. Bruce, Science 337 (2012) 563–566.
[91] D. Lin, Y. Liu, Y. Cui, Nat. Nanotechnol. 12 (2017) 194.
[92] F. Wu, Y.-X. Yuan, X.-B. Cheng, Y. Bai, Y. Li, C. Wu, Q. Zhang, Energy Storage Mater 15 (2018) 148–170.
[93] J. Yi, J. Chen, Z. Yang, Y. Dai, W. Li, J. Cui, F. Ciucci, Z. Lu, C. Yang, Adv. Energy Mater. 9 (2019) 1901796.
[94] K. Yan, Z. Lu, H.-W. Lee, F. Xiong, P.-C. Hsu, Y. Li, J. Zhao, S. Chu, Y. Cui, Nat. Energy 1 (2016) 16010.
[95] T. Yang, T. Qian, X. Shen, M. Wang, S. Liu, J. Zhong, C. Yan, F. Rosei, J. Mater. Chem. A 7 (2019) 14496–14503.
[96] Y. Sun, J. Zhou, H. Ji, J. Liu, T. Qian, C. Yan, ACS Appl. Mater. Interfaces 11 (2019) 32008–32014.
[97] J. Gu, Q. Zhu, Y. Shi, H. Chen, D. Zhang, Z. Du, S. Yang, ACS Nano 14 (2020) 891–898.
[98] J. Yu, Y.-Q. Lyu, J. Liu, M.B. Effat, S.C.T. Kwok, J. Wu, F. Ciucci, J. Mater. Chem. A 7 (2019) 17995–18002.
[99] H. Al Salem, G. Babu, C.V. Rao, L.M.R. Arava, J. Am. Chem. Soc. 137 (2015) 11542–11545.
[100] Z. Li, C. Li, X. Ge, J. Ma, Z. Zhang, Q. Li, C. Wang, L. Yin, Nano Energy 23 (2016) 15–26.
[101] M. Liu, N. Deng, J. Ju, L. Wang, G. Wang, Y. Ma, W. Kang, J. Yan, ACS Appl. Mater. Interfaces 11 (2019) 17843–17852.
[102] X. Liang, C. Hart, Q. Pang, A. Garsuch, T. Weiss, L.F. Nazar, Nat. Commun. 6 (2015) 5682.
[103] G. Babu, N. Masurkar, H. Al Salem, L.M.R. Arava, J. Am. Chem. Soc. 139 (2017) 171–178.
[104] Z. Sun, J. Zhang, L. Yin, G. Hu, R. Fang, H.-M. Cheng, F. Li, Nat. Commun. 8 (2017) 14627.
[105] Z. Du, X. Chen, W. Hu, C. Chuang, S. Xie, A. Hu, W. Yan, X. Kong, X. Wu, H. Ji, L.-J. Wan, J. Am. Chem. Soc. 141 (2019) 3977–3985.
[106] K. Zhang, Z. Chen, R. Ning, S. Xi, W. Tang, Y. Du, C. Liu, Z. Ren, X. Chi, M. Bai, C. Shen, X. Li, X. Wang, X. Zhao, K. Leng, S.J. Pennycook, H. Li, H. Xu, K.P. Loh, K. Xie, ACS Appl. Mater. Interfaces 11 (2019) 25147–25154.
[107] Z. Shi, L. Wang, H. Xu, J. Wei, H. Yue, H. Dong, Y. Yin, S. Yang, Chem. Commun. 55 (2019) 12056–12059.

[108] N. Yabuuchi, K. Kubota, M. Dahbi, S. Komaba, Chem. Rev. 114 (2014) 11636–11682.
[109] J. Wu, Z. Lu, K. Li, J. Cui, S. Yao, M. Ihsan-ul Haq, B. Li, Q.-H. Yang, F. Kang, F. Ciucci, J.-K. Kim, J. Mater. Chem. A 6 (2018) 5668–5677.
[110] K.B. Hueso, M. Armand, T. Rojo, Energy Environ. Sci. 6 (2013) 734–749.
[111] Y. Li, G. Chen, J. Mou, Y. Liu, S. Xue, T. Tan, W. Zhong, Q. Deng, T. Li, J. Hu, C. Yang, K. Huang, M. Liu, Energy Storage Mater 28 (2020) 196–204.
[112] Y. Li, P. Zhou, H. Li, T. Gao, L. Zhou, Y. Zhang, N. Xiao, Z. Xia, L. Wang, Q. Zhang, L. Gu, S. Guo, Small Methods 4 (2020) 1900701.
[113] C. Wang, H. Song, C. Yu, Z. Ullah, Z. Guan, R. Chu, Y. Zhang, L. Zhao, Q. Li, L. Liu, J. Mater. Chem. A 8 (2020) 3421–3430.
[114] J. Wu, J. Chen, Y. Huang, K. Feng, J. Deng, W. Huang, Y. Wu, J. Zhong, Y. Li, Sci. Bull. 64 (2019) 1875–1880.
[115] Y. Li, H. Dai, Chem. Soc. Rev. 43 (2014) 5257–5275.
[116] Z. Lyu, Y. Zhou, W. Dai, X. Cui, M. Lai, L. Wang, F. Huo, W. Huang, Z. Hu, W. Chen, Chem. Soc. Rev. 46 (2017) 6046–6072.
[117] C. Tang, B. Wang, H.-F. Wang, Q. Zhang, Adv. Mater. 29 (2017) 1703185.
[118] J. Han, X. Meng, L. Lu, J. Bian, Z. Li, C. Sun, Adv. Funct. Mater. 29 (2019) 1808872.
[119] J. Li, S. Chen, N. Yang, M. Deng, S. Ibraheem, J. Deng, J. Li, L. Li, Z. Wei, Angew. Chem. Int. Ed. 58 (2019) 7035–7039.
[120] D. Liu, B. Wang, H. Li, S. Huang, M. Liu, J. Wang, Q. Wang, J. Zhang, Y. Zhao, Nano Energy 58 (2019) 277–283.
[121] Z. Lu, B. Wang, Y. Hu, W. Liu, Y. Zhao, R. Yang, Z. Li, J. Luo, B. Chi, Z. Jiang, M. Li, S. Mu, S. Liao, J. Zhang, X. Sun, Angew. Chem. Int. Ed. 58 (2019) 2622–2626.
[122] B. Wang, X. Wang, J. Zou, Y. Yan, S. Xie, G. Hu, Y. Li, A. Dong, Nano Lett. 17 (2017) 2003–2009.
[123] W. Zang, A. Sumboja, Y. Ma, H. Zhang, Y. Wu, S. Wu, H. Wu, Z. Liu, C. Guan, J. Wang, S.J. Pennycook, ACS Catal. 8 (2018) 8961–8969.
[124] L. Ma, S. Chen, Z. Pei, Y. Huang, G. Liang, F. Mo, Q. Yang, J. Su, Y. Gao, J. A. Zapien, C. Zhi, ACS Nano 12 (2018) 1949–1958.
[125] J. Wang, W. Liu, G. Luo, Z. Li, C. Zhao, H. Zhang, M. Zhu, Q. Xu, X. Wang, C. Zhao, Y. Qu, Z. Yang, T. Yao, Y. Li, Y. Lin, Y. Wu, Y. Li, Energy Environ. Sci. 11 (2018) 3375–3379.
[126] W. Xiang, Y. Zhao, Z. Jiang, X. Li, H. Zhang, Y. Sun, Z. Ning, F. Du, P. Gao, J. Qian, K. Kato, M. Yamauchi, Y. Sun, J. Mater. Chem. A 6 (2018) 23366–23377.
[127] L. Yang, L. Shi, D. Wang, Y. Lv, D. Cao, Nano Energy 50 (2018) 691–698.
[128] Y. Chen, S. Ji, S. Zhao, W. Chen, J. Dong, W.-C. Cheong, R. Shen, X. Wen, L. Zheng, A.I. Rykov, S. Cai, H. Tang, Z. Zhuang, C. Chen, Q. Peng, D. Wang, Y. Li, Nat. Commun. 9 (2018) 5422.
[129] W. Xie, Y. Song, S. Li, J. Li, Y. Yang, W. Liu, M. Shao, M. Wei, Adv. Funct. Mater. 29 (2019) 1906477.
[130] B.-Q. Li, C.-X. Zhao, S. Chen, J.-N. Liu, X. Chen, L. Song, Q. Zhang, Adv. Mater. 31 (2019) 1900592.
[131] J. Zhang, M. Zhang, Y. Zeng, J. Chen, L. Qiu, H. Zhou, C. Sun, Y. Yu, C. Zhu, Z. Zhu, Small 15 (2019) 1900307.
[132] R. Van Hardeveld, F. Hartog, Surf. Sci. 15 (1969) 189–230.
[133] N. Lopez, T.V.W. Janssens, B.S. Clausen, Y. Xu, M. Mavrikakis, T. Bligaard, J. K. Nørskov, J. Catal. 223 (2004) 232–235.
[134] M. Valden, X. Lai, D.W. Goodman, Science 281 (1998) 1647–1650.
[135] J. Li, X. Li, H.-J. Zhai, L.-S. Wang, Science 299 (2003) 864–867.
[136] B. Yoon, H. Häkkinen, U. Landman, A.S. Wörz, J.-M. Antonietti, S. Abbet, K. Judai, U. Heiz, Science 307 (2005) 403–407.
[137] M. Boronat, A. Leyva-Pérez, A. Corma, Acc. Chem. Res. 47 (2014) 834–844.
[138] L. Liu, A. Corma, Chem. Rev. 118 (2018) 4981–5079.
[139] H. Xu, D. Cheng, D. Cao, X.C. Zeng, Nat. Catal. 1 (2018) 339–348.
[140] G. Zhou, S. Zhao, T. Wang, S.-Z. Yang, B. Johannessen, H. Chen, C. Liu, Y. Ye, Y. Wu, Y. Peng, C. Liu, S.P. Jiang, Q. Zhang, Y. Cui, Nano Lett. 20 (2020) 1252–1261.
[141] Q. Zhang, Y. Wang, Z.W. Seh, Z. Fu, R. Zhang, Y. Cui, Nano Lett. 15 (2015) 3780–3786.
[142] C. Zhu, S. Fu, Q. Shi, D. Du, Y. Lin, Angew. Chem. Int. Ed. 56 (2017) 13944–13960.

Zhiqi Zhang received his Bachelor's degree and Master's degree from Northeastern University and PhD degree in chemistry from Nanjing University. He is currently a postdoctoral fellow in the Department of Mechanical and Aerospace Engineering at The Hong Kong University of Science and Technology. His research interest mainly focuses on energy nanomaterials and their applications in energy storage and conversion.

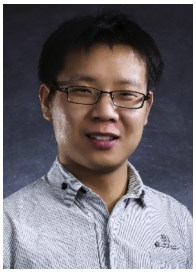

Jiapeng Liu received his B.Eng. from Northwestern Polytechnical University. Currently, he is a Ph.D. student in the Department of Mechanical and Aerospace Engineering at The Hong Kong University of Science and Technology. His research interest mainly focuses on theoretical study of energy-related materials using density functional theory as well as machine learning techniques.

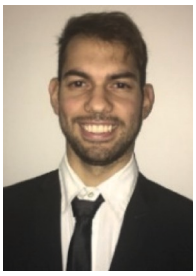

Antonino Curcio received a dual B.Sc. degree from Politecnico di Milano, Italy, and TongJi University, China, as well as a M. Sc. degree from Politecnico di Milano. Currently, he is pursuing his Ph.D. in Mechanical and Aerospace Engineering at The Hong Kong University of Science and Technology under the auspices of the Hong Kong Ph.D. fellowship. His main scientific interest is in advanced materials for electrochemical energy conversion and storage. His current research projects involve the study of electrocatalysts for the oxygen evolution reaction, oxygen reduction reaction, and hydrogen evolution reaction.

Yuhao Wang obtained his master degree in Chemical and Biomolecular Engineering from the Hong Kong University of Science and Technology in 2019. He is a research assistant in the Department of Mechanical and Aerospace Engineering at The Hong Kong University of Science and Technology. His current research focuses on solid oxide cells, electrocatalysis, and energy storage materials.

Junxiong Wu received his B.E. from Fuzhou University and MS from Tsinghua University. Currently, he is a PhD student in the Department of Mechanical and Aerospace Engineering at The Hong Kong University of Science and Technology under joint supervision of Prof. Francesco Ciucci and Prof. Jang-Kyo Kim. His research focuses on new materials for sodium-ion and sodium-metal batteries.

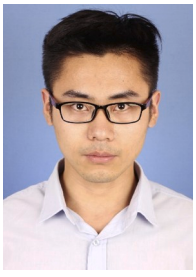

Guodong Zhou received his B.Eng. and M.Eng. from Zhejiang University. Currently, he is a PhD student in the Department of Mechanical and Aerospace Engineering at The Hong Kong University of Science and Technology under the supervision of Prof. Francesco Ciucci. His research focuses on new electrolytes for lithium-ion batteries and lithium metal batteries.

Dr. Zhenghua Tang currently is an associate professor of New Energy Research Institute at South China University of Technology. He is also the recipient of Guangdong Natural Science Funds for Distinguished Young Scholar. He obtained his BS degree at Lanzhou University in 2005, and his PhD degree at Georgia State University in 2012. After two years' postdoctoral training at University of Miami, he started his current position since 2014. His research focuses on controllable synthesis and electrocatalytic applications of atomically precise metal nanocluster and single-atom based nanomaterials.

Francesco Ciucci is an Associate Professor at The Hong Kong University of Science and Technology. He obtained his PhD from the California Institute of Technology, USA, and did his postdoctoral work at the University of Heidelberg, Germany. Francesco's current research centers on solid-state energy technologies, including solid-oxide fuel cells, electrolyzers, and solid-state batteries, with particular emphasis on the modeling of these systems and the development of new functional materials.